in inflamed lymph nodes enhances dendritic cell mobilization. *Immunity.* 2006;24(2):203–215.
44. Harrell MI, Iritani BM, Ruddell A. Tumor-induced sentinel lymph node lymphangiogenesis and increased lymph flow precede melanoma metastasis. *Am J Pathol.* 2007;170(2):774–786.
45. Carr I. Lymphatic metastasis. *Cancer Metastasis Rev.* 1983;2(3):307–317.
46. Azzali G. Tumor cell transendothelial passage in the absorbing lymphatic vessel of transgenic adenocarcinoma mouse prostate. *Am J Pathol.* 2007;170(1):334–346.
47. Yang J, et al. Twist, a master regulator of morphogenesis, plays an essential role in tumor metastasis. *Cell.* 2004;117(7):927–939.
48. Tang DG, Bhatia B, Tang S, Schneider-Broussard R. 15-lipoxygenase 2 (15-LOX2) is a functional tumor suppressor that regulates human prostate epithelial cell differentiation, senescence and growth (size). *Prostaglandins Other Lipid Mediat.* 2007;82(1–4):135–146.
49. Brash AR, Boeglin WE, Chang MS. Discovery of a second 15S-lipoxygenase on humans. *Proc Natl Acad Sci U S A.* 1997;94(12):6148–6152.
50. Jiang WG, Douglas-Jones A, Mansell RE. Levels of expression of lipoxygenases and cycloxygenase 2 in human breast cancer. *Prostaglandins Leukot Essent Fatty Acids.* 2003;69(4):275–281.
51. Bhattacharya S, Mathew G, Jayne DG, Pelengaris S, Khan M. 15-lipoxygenase-1 in colorectal cancer: a review. *Tumour Biol.* 2009;30(4):185–199.
52. Honn KV, et al. Enhanced endothelial cell retraction mediated by 12(S)-HETE: a proposed mechanism for the role of platelets in tumor cell metastasis. *Exp Cell Res.* 1994;210(1):1–9.
53. Uchide K, Sakon M, Ariyoshi H, Nakamori S, Tokunaga M, Monden M. Cancer cells cause vascular endothelial cell (vEC) retraction via 12(S)HETE secretion; the possible role of cancer cell derived microparticle. *Ann Surg Oncol.* 2007;14(2):862–868.
54. Moreno JJ. New aspects of the role of hydroxyeicosatetraenoic acids in cell growth and cancer development. *Biochem Pharmacol.* 2009;77(1):1–10.
55. Kim GY, Lee JW, Cho SH, Seo JM, Kim JH. Role of the low-affinity leukotriene B4 receptor BLT2 in VEGF-induced angiogenesis. *Arterioscler Thromb Vasc Biol.* 2009;29(6):915–920.
56. Guo Y, Nie D, Honn KV. Cloning and identification of a G-protein coupled receptor for 12(S)-HETE. *Proc Amer Assoc Cancer Res.* 2004;45:2746.
57. Neve RM, et al. A collection of breast cancer cell lines for the study of functionally distinct cancer subtypes. *Cancer Cell.* 2006;10(6):515–527.
58. Umezawa K. Inhibition of experimental metastasis by enzyme inhibitors from microorganisms and plants. *Adv Enzyme Regul.* 1996;36:267–81.
59. Tong WG, Ding XZ, Adrian TE. The mechanisms of lipoxygenase inhibitor-induced apoptosis in human breast cancer cells. *Biochem Biophys Res Commun.* 2002;296(4):942–948.
60. Russo J, et al. The concept of stem cell in the mammary gland and its implication in morphogenesis, cancer and prevention. *Front Biosci.* 2006; 11:151–172.
61. Charafe-Jauffret E, Monville F, Ginestier C, Dontu G, Birnbaum D, Wicha MS. Cancer stem cells in breast: current opinion and future challenges. *Pathobiology.* 2008;75(2):75–84.
62. Wick N, et al. Lymphatic precollectors contain a novel, specialized subpopulation of podoplanin low, CCL27-expressing lymphatic endothelial cells. *Am J Pathol.* 2008;173(4):1202–1209.
63. Vinatzer U, et al. Expression of HER2 and the coamplified genes GRB7 and MLN64 in human breast cancer: quantitative real-time reverse transcription-PCR as a diagnostic alternative to immunohistochemistry and fluorescence in situ hybridization. *Clin Cancer Res.* 2005;11(23):8348–8357.
64. Kriehuber E, et al. Isolation and characterization of dermal lymphatic and blood endothelial cells reveal stable and functionally specialized cell lineages. *J Exp Med.* 2001;194(6):797–808.
65. Werz O, Steinhilber D. Selenium-dependent peroxidases suppress 5-lipoxygenase activity in B-lymphocytes and immature myeloid cells. The presence of peroxidase-insensitive 5-lipoxygenase activity in differentiated myeloid cells. *Eur J Biochem.* 1996;242(1):90–97.

JAPANESE DERMATOLOGICAL ASSOCIATION
THE JOURNAL OF DERMATOLOGY

doi: 10.1111/j.1346-8138.2011.01396.x

Journal of Dermatology 2012; **39**: 366–374

ORIGINAL ARTICLE

Targeted overexpression of Angptl6/angiopoietin-related growth factor in the skin promotes angiogenesis and lymphatic vessel enlargement in response to ultraviolet B

Hidenori OKAZAKI,[1] Satoshi HIRAKAWA,[2] Masachika SHUDOU,[3] Yoshiki NAKAOKA,[1] Yuji SHIRAKATA,[1] Keishi MIYATA,[4,5] Yuichi OIKE,[4] Koji HASHIMOTO,[1] Koji SAYAMA[1]

[1]*Department of Dermatology, Ehime University Graduate School of Medicine, Ehime,* [2]*Department of Dermatology, Hamamatsu University School of Medicine, Shizuoka,* [3]*Department of Bioscience, Ehime University, Ehime,* [4]*Departments of Molecular Genetics, and* [5]*Immunology, Allergy and Vascular Medicine, Graduate School of Medical Sciences, Kumamoto University, Kumamoto, Japan*

ABSTRACT

Angiogenesis is required for physiological tissue repair processes, such as cutaneous wound healing. However, recent studies indicate that endogenous angiogenic factors may enhance photo-induced skin alterations in response to experimental ultraviolet (UV)-B exposure. Angiopoietin-related growth factor (AGF), also known as angiopoietin-like protein 6 (Angptl6), is known to promote new blood vessel formation and vascular hyperpermeability. Importantly, epidermal overexpression of Angptl6/AGF in mice promotes wound healing in the skin. However, it remains unclear whether overexpression of Angptl6/AGF facilitates tissue repair processes in response to UV-B irradiation. To test this hypothesis, we subjected *Angptl6/AGF* transgenic mice to acute or chronic UV-B exposure. Surprisingly, transgenic mice showed enhanced photosensitivity to subthreshold doses of UV-B that did not induce skin alterations in wild-type littermates. Marked enlargement of blood vessels was observed after a single exposure to UV-B in *Angptl6/AGF* transgenic mice, although no epidermal changes were observed. Chronic UV-B exposure over 14 weeks promoted cutaneous skin damage in *Angptl6/AGF* transgenic mice, whereas wild-type mice showed little or no macroscopic skin alteration. In addition to pronounced angiogenesis and epidermal hyperplasia, marked enlargement of dermal lymphatic vessels was observed in UV-B-exposed *Angptl6/AGF* transgenic mice. Electron microscopy analysis further revealed that the number and size of collagen bundles in the dermis was markedly reduced after chronic UV-B exposure in *Angptl6/AGF* transgenic mice. Taken together, these results indicate that ectopic expression of Angptl6/AGF in mice likely promotes UV-B-induced skin alterations, and that angiogenesis could be a therapeutic target in prevention of skin photo-aging.

Key words: collagen, photoaging, photosensitivity, transgenic mice, vascular endothelial growth factor.

INTRODUCTION

Angiogenesis – the formation of new blood vessels from pre-existing ones – is induced in physiological tissue repair and in pathological conditions such as cutaneous inflammation and/or tumor progression.[1,2] Ultraviolet (UV)-B induces acute and chronic skin alterations. Acute exposure of human or mouse skin to UV-B promotes erythema and/or blisters because of marked increases in vascular permeability. UV-B-induced skin damage is characterized by epidermal hyperplasia, degradation of matrix proteins and dermal elastosis.[3] Previous studies have shown that pronounced angiogenesis is induced by acute UV-B irradiation of human and mouse skin.[4,5] In fact, UV-B irradiation upregulates potent angiogenic factors in the skin, including vascular endothelial growth factor (VEGF)-A, basic fibroblast growth factor and interleukin-8.[6–8] Overexpression of VEGF-A in the epidermis has also been shown to induce enhanced photosensitivity in the skin in response to a single UV-B exposure.[9] In contrast, systemic blockade of endogenous VEGF-A signaling significantly reduces photosensitivity and antagonizes enlargement of blood vessels in the skin, indicating that the primary angiogenic response may be the crucial event that facilitates acute photo-induced skin reactions. Importantly, chronic UV-B exposure caused prominent wrinkle formation in VEGF-A transgenic mice by promoting significant new blood vessel formation in the skin, leading to the idea that endogenous angiogenic factors such as VEGF-A function to promote photo-induced skin damage. Currently, it is unclear whether ectopic expression of angiogenic growth factors contributes to cutaneous tissue repair processes in response to UV-B exposure.

Angiopoietin-related growth factor (AGF), also known as Angptl6, is a member of the family of angiopoietin-like proteins, which play crucial roles in murine vascular development and/or physiological

Correspondence: Satoshi Hirakawa, M.D., Ph.D., Department of Dermatology, Hamamatsu University School of Medicine, 1-20-1 Handayama, Higashi-ku, Hamamatsu-shi, Shizuoka 431-3192, Japan. Email: hirakawa@hama-med.ac.jp
Received 17 July 2011; accepted 25 July 2011.

metabolism.[10,11] Like all angiopoietins, Angptl6/AGF possesses an N-terminal coiled-coil domain and a C-terminal fibrinogen-like domain.[12] Most angiopoietins are known to bind Tie1 and/or Tie2 receptors, whereas Angptl6/AGF remains an orphan ligand. Targeted disruption of *Angptl6/AGF* in mice leads to obesity and insulin resistance, reflecting clinical features reminiscent of human metabolic syndrome.[11] Meanwhile, targeted overexpression of Angptl6/AGF in mouse skin promotes angiogenesis and epidermal hyperplasia, indicating that Angptl6/AGF mediates pleiotropic effects towards several cell lineages, including epidermal keratinocytes.[10,13] Of particular interest, Angptl6/AGF transgenic mice in the skin show markedly enhanced cutaneous wound healing during the tissue repair process compared to wild-type mice.[13] Importantly, little or no Angptl6/AGF is expressed endogenously in mouse skin, indicating that Angptl6/AGF has a potent tissue repair function separate from its role as an angiogenic factor in the skin.

Recent studies indicate that lymphatic vessels play a crucial role in mediating UV-B-induced cutaneous changes.[14] UV-B exposure induces marked enlargement of lymphatic vessels in mouse skin. Sufficient lymphatic flow is required to suppress dermal edema and inflammation in response to a single UV-B exposure. Importantly, activation of VEGF-C/vascular endothelial growth factor receptor-3, one of the major pathways promoting lymphatic vessel growth and function,[15] has been shown to attenuate UV-B-induced edema formation and skin inflammation.[16] Furthermore, lymphatic vessels show enhanced leakiness in UV-B-irradiated skin, leading to reduced lymphatic drainage and impaired function.[14] Moreover, among Angptl family members, targeted Angptl2 overexpression in the skin has been recently shown to promote enlargement of dermal lymphatic as well as blood vessels.[17] Currently, it is unclear whether Angptl6/AGF alters the growth of lymphatic vessels in experimental mouse models of UV-B exposure.

Here, to test the hypothesis whether AGF facilitates cutaneous tissue repair processes in response to UV-B irradiation, we subjected *Angptl6/AGF* transgenic mice to either acute or chronic UV-B exposure. We report that overexpression of Angptl6/AGF in mouse skin enhances photosensitivity to acute UV-B exposure by promoting enlargement of dermal blood vessels but does not induce epidermal hyperplasia in response to a minimal erythema dose of UV-B. By contrast, chronic UV-B exposure, at a dose that did not induce detectable skin changes in wild-type mice, induced pronounced angiogenesis and enlargement of lymphatic vessels, leading to wrinkle development in *Angptl6/AGF* transgenic mice. Together, these results indicate that targeted overexpression of Angptl6/AGF in mouse skin may prevent photo-induced cutaneous damage from a single exposure of UV-B, but long-term AGF induction could mediate UV-B-induced skin alterations such as photo-induced skin aging.

METHODS

UV-B irradiation regime

Ten-week-old male FVB/N or BALB/c wild-type mice, or keratin 14 promoter-driven *Angptl6/AGF* transgenic mice were exposed to graded doses of four equally charged fluorescent lamps (ULTRAVIOLET-B TL 20W/12RS; Philips, Amsterdam, Netherlands). The minimal erythema dose (MED) was determined by irradiation of square areas on back skin with seven different doses of UV-B, ranging 5.0×10^{-2} to 4.0×10^{-1} J/cm^2 (n = 5/group). An additional skin area was sham-irradiated. Erythema formation was evaluated 48 h after irradiation. Ten-week-old male BALB/c wild-type mice or transgenic overexpressing Angptl6/AGF in the epidermis under control of the human keratin 14 promoter were exposed to seven different UV-B doses, ranging 3.0×10^{-2} to 9.0×10^{-2} J/cm^2, on the dorsal skin (n = 5/group) to determine MED. In addition, ear skin of AGF transgenic mice and wild-type littermates was exposed to a single dose of UV-B by 9.0×10^{-2} J/cm^2 (n = 5/group). Thereafter, ear thickness was measured daily for up to 8 days. In an additional experiment, 8-week-old male wild-type or AGF transgenic mice were irradiated three times weekly for 14 weeks with a total dose of 8.185 J/cm^2 (n = 10/genotype). Control mice were sham-irradiated. Skin samples were either snap-frozen with O.C.T.-Compound (Sakura Finetek Japan, Tokyo, Japan) in ethanol dry ice or fixed in 4% paraformaldehyde in phosphate-buffered saline. All animal studies were approved by the Ehime University Subcommittee on Research Animal Care.

Real-time reverse transcription polymerase chain reaction (RT–PCR)

Total RNA was isolated from dorsal skin of *Angptl6/AGF* transgenic mice or wild-type littermates (n = 5) and of five non-irradiated control mice using Isogen (Wako, Osaka, Japan). Real-time RT–PCR was performed and analyzed with a 7900 HT Fast Real-Time PCR System (Applied Biosystems, Branchburg, NJ, USA). Primers and probes for β-actin, AGF, VEGF-A, VEGF-C and VEGF-D were purchased from Applied Biosystems. RNA analysis was carried out using a TaqMan RT–PCR Master Mix reagents kit (Applied Biosystems), according to the manufacturer's protocol. Target gene expression in test samples was normalized to corresponding β-actin expression.

Histological analysis and immunofluorescence stains

Immunofluorescence was analyzed on 5-μm frozen sections, as described previously,[18] using a biotinylated rat antimouse CD31 antibody (BD Biosciences Pharmingen, San Diego, CA, USA), a monoclonal rat LYVE-1 antibody (MBL, Nagoya, Japan), and corresponding secondary antibodies labeled with Alexa Fluor 488 or 594 (Molecular Probes, Eugene, OR, USA). Representative sections were prepared from skin of UV-B- or sham-irradiated mice (n = 5/group). Nuclei were counterstained with 4′,6′-diamidino-2-phenylindole dihydrochloride (DAPI; Molecular Probes). Staining was analyzed and digital images were captured using a confocal laser scanning microscope LSM510 (Carl Zeiss, Jena, Germany). Morphometric analyses were performed using IP-LAB software as described previously.[19] In addition, paraffin sections were prepared from skin of the same mice. Routine hematoxylin–eosin or Masson-trichrome staining was performed.

Computer-assisted morphometric vessel analysis

Double immunofluorescence staining using anti-CD31 antibody for blood vessels and anti-LYVE-1 antibody for lymphatic vessels was analyzed using an LSM510 microscope. Representative fields of

each section were examined at ×10 magnification, and the number of vessels/mm^2, average vessel size and relative area occupied by blood or lymphatic vessels were determined in a dermal area within 200 μm of the epidermal–dermal junction. An unpaired Student's *t*-test was used to analyze differences in microvessel density, vascular size and relative vascular area.

Transmission electron microscopy analysis

Skin tissues were fixed in 0.1 mol/L phosphate-buffered 2.5% glutaraldehyde with 0.1% tannic acid (pH 7.4) for 2 h, and postfixed with 1% osmium tetroxide in phosphate buffer for 2 h. Specimens were washed in 0.25 mol/L sucrose solution, dehydrated in a graded ethanol series, and embedded in an Epon resin mixture (Epon 812 resin; TAAB Laboratories Equipment, Aldermaston, Berks, England). Ultra-thin sections of 60–80 nm were prepared using an Ultracut S blade (Leica Microsystems, Wetzlar, Germany) and subsequently double-stained with uranyl acetate and lead citrate. Specimens were analyzed at a voltage of 80 kV, and images were captured using a transmission electron microscope, JEM-1230 (JEOL, Tokyo, Japan).

RESULTS

BALB/c and FVB/N wild-type mice show comparable MED

Transgenic mice in which Angptl6/AGF is driven from the keratin 14 promoter (*K14–Angptl6/AGF*) were originally bred on a BALB/c background.[13] However, previous studies of the role of angiogenesis in mediating UV-B-induced skin alterations in transgenic mice have utilized mice on an FVB/N background.[4,9] Therefore, to assess the biological effect of Angptl6/AGF upon photodamaged skin, we first compared the MED of wild-type FVB/N and BALB/c mice using graded UV-B doses. The dorsal skin of FVB/N wild-type mice showed signs of erythema 48 h after irradiation with 7.2×10^{-2} J/cm^2 UV-B or higher doses (n = 6) (Fig. 1a). Similarly, BALB/c wild-type mice developed minimal erythema on back skin at a dose of 7.2×10^{-2} J/cm^2 UV-B (n = 6) (Fig. 1b) in the same timeframe. Therefore, both FVB/N and BALB/c wild-type mice showed comparable erythema formation at the same radiation dose, indicating that BALB/c mice are suitable models to evaluate photosensitivity following UV-B radiation.

Cutaneous photosensitivity is enhanced in *Angptl6/AGF* transgenic mice

To determine whether epidermal Angptl6/AGF overexpression alters cutaneous photosensitivity in the skin, we evaluated MED of *Angptl6/AGF* transgenic mice by exposing them to doses of UV-B ranging 3.0×10^{-2} to 9.0×10^{-2} J/cm^2. The dorsal skin of AGF transgenic mice showed signs of erythema at 4.0×10^{-2} J/cm^2 UV-B and higher (n = 5) (Fig. 1d), whereas in comparably-treated wild-type littermates the MED was defined as 7.2×10^{-2} J/cm^2 UV-B (Fig. 1c). Statistical analysis showed that the MED for *Angptl6/AGF* transgenic mice is significantly lower than that of wild-type mice (Fig. 1e). Overall, these observations suggest that Angptl6/AGF transgenic mice show enhanced cutaneous photosensitivity relative to wild-type mice.

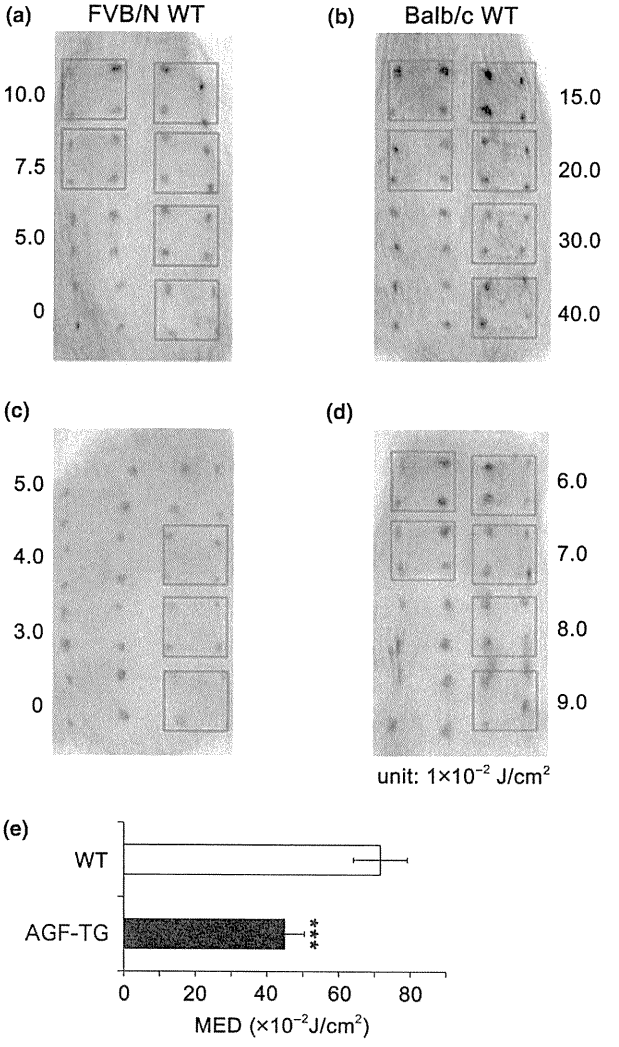

Figure 1. Enhanced photosensitivity of *Angptl6/AGF* transgenic (TG) mice. (a,b) The dorsal skin was exposed to graded doses of ultraviolet (UV)-B ranging 5.0×10^{-2} to 4×10^{-1} J/cm^2, or to sham irradiation. A minimal erythema dose (MED) of 7.5×10^{-2} J/cm^2 was determined by analyzing skin of wild-type (WT) FVB/N mice 48 h after irradiation (a, n = 5). A comparable MED was observed in wild-type BALB/c mice (b, n = 5). (c,d) Analysis of the skin of *Angptl6/AGF* transgenic mice indicated a MED of 4.0×10^{-2} J/cm^2 of UV-B (d, n = 5), whereas skin of wild-type littermates showed signs of erythema at 7.0×10^{-2} J/cm^2. (e, n = 5) Statistical analysis confirmed that the MED for *Angptl6/AGF* transgenic mice is significantly lower than that of wild-type mice. Data are expressed as mean ± standard deviation (n = 6/condition). ***$P < 0.001$.

Angptl6/AGF promotes blood vessel enlargement in response to a single UV-B exposure

One MED induces formation of an erythema characterized by microvascular enlargement in the skin. Therefore, we asked whether macroscopic vascular enlargement occurs in the skin of *Angptl6/AGF* transgenic mice by irradiating them with increased doses of UV-B. A dose of 9.0×10^{-2} J/cm^2 UV-B induced macroscopic

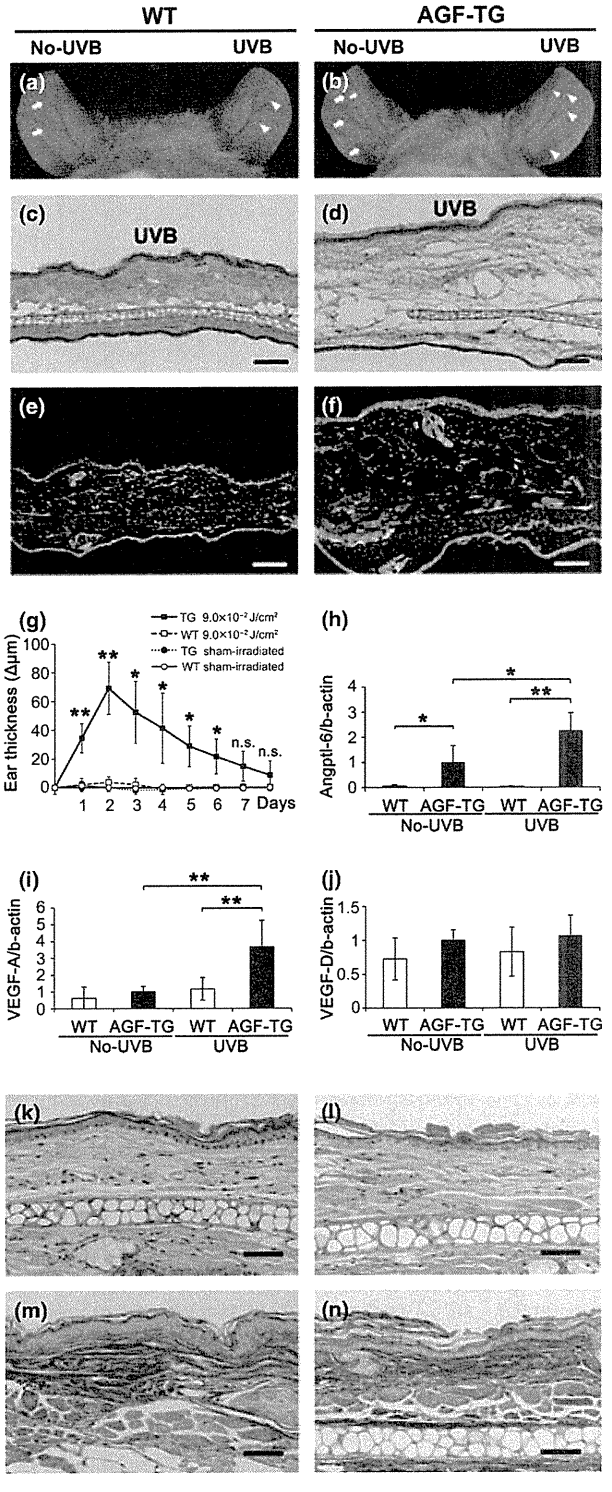

Figure 2. Angptl6/AGF promotes blood vessel enlargement following acute ultraviolet (UV)-B irradiation (a,b). The ear skin of *Angptl6/AGF* transgenic (TG) mice or wild-type (WT) littermates was exposed to a single irradiation of UV-B of 9.0×10^{-2} J/cm^2. Forty-eight hours later, transgenic mice developed erythema and enlargement of blood vessels (b, arrowheads) relative to sham-irradiated ears (b, arrows), whereas little or no alteration was observed in UV-B-exposed (a, arrowheads) or sham-irradiated ear skin of wild-type mice (a, arrows). (c,d) Histological analysis revealed that ear skin of wild-type mice appeared normal (c, hematoxylin–eosin [HE]), whereas the skin of Angptl6/AGF-overexpressing mice showed dermal edema and vessel dilation particularly on the side of UV-B irradiation as compared with the other side of ear skin which is unexposed to UV-B (d, HE). (e,f) Double immunofluorescence staining reveals dilated CD31$^+$ blood vessels (red) in transgenic mice, while no such changes were seen in skin of wild-type littermates. LYVE-1$^+$ stain (green) was comparable between ear skin of AGF transgenic mice and wild-type littermates. Nuclei are stained blue (4′,6′-diamidino-2-phenylindole dihydrochloride [DAPI] stain). (Scale bars, 100 μm.) (g) Angptl6/AGF-overexpressing mice show significant ear swelling 48 h after irradiation with 9.0×10^{-2} J/cm^2 UV-B (◆), while no ear swelling is observed in similarly treated wild-type littermates (■). (h–j) Quantitative reverse transcription polymerase chain reaction (RT–PCR) analyses of ear skin of Angptl6/AGF-overexpressing mice and wild-type littermates 48 h after UV-B irradiation (n = 5). Increased Angptl6/AGF and vascular endothelial growth factor (VEGF)-A expression was seen in K14–*Angptl6/AGF* mice in response to a single UV-B exposure (h,i). Comparable levels of VEGF-D mRNA were seen in the presence or absence of UV-B irradiation (j). Routine HE stain showed that ear skin of Angptl6/AGF-overexpressing mice and wild-type mice appeared comparable and normal 8 days after UV-B irradiation (k,l). Azan–Mallory staining showed that collagen bundles in the papillary dermis remained normal in UV-B-treated *Angptl6/AGF* transgenic mice (n) and wild-type littermates 8 days after UV-B irradiation (m). Data are expressed as means ± standard deviation (n = 5/condition and time point). $^{**}P < 0.01$; $^{*}P < 0.05$.

vascular enlargement in ear skin of *Angptl6/AGF* transgenic mice (Fig. 2b, arrowheads) as compared with sham-irradiated ears (Fig. 2b, arrows), whereas no macroscopic vascular alteration was seen in UV-B-exposed (Fig. 2a, arrowheads) or sham-irradiated ear skin of wild-type littermates (Fig. 2a, arrows). Histologically, ear skin of *Angptl6/AGF* transgenic mice showed marked edema in the dermis and vessel dilation 48 h after irradiation (Fig. 2d), whereas the skin of wild-type mice showed no significant changes at 9.0×10^{-2} J/cm^2 UV-B (Fig. 2c). Double immunofluorescence with antibodies against CD31 for blood vessels and LYVE-1 for lymphatic vessels showed that blood vessels were markedly enlarged in *Angptl6/AGF* transgenic mice (Fig. 2f), whereas no such changes were seen in wild-type littermates (Fig. 2e). Lymphatic vessels in *Angptl6/AGF* transgenic mice remained normal as well as lymphatic vessels in wild-type littermates. Furthermore, *Angptl6/AGF* transgenic mice showed prominent, albeit transient, ear swelling 48 h after irradiation (Fig. 2g). In contrast, the ears of wild-type mice showed no detectable changes in thickness after a single UV-B irradiation at 9.0×10^{-2} J/cm^2 (Fig. 2g).

Quantitative real-time RT–PCR analyses of RNA extracted from mouse ears showed that expression levels of Angptl6/AGF and VEGF-A increased by 2.0-fold (Fig. 2h) and 2.5-fold (Fig. 2i), respectively, in *Angptl6/AGF* transgenic mice 48 h after irradiation. By contrast, wild-type mice showed little or no change in expression levels of either transcript after irradiation with 9.0×10^{-2} J/cm^2

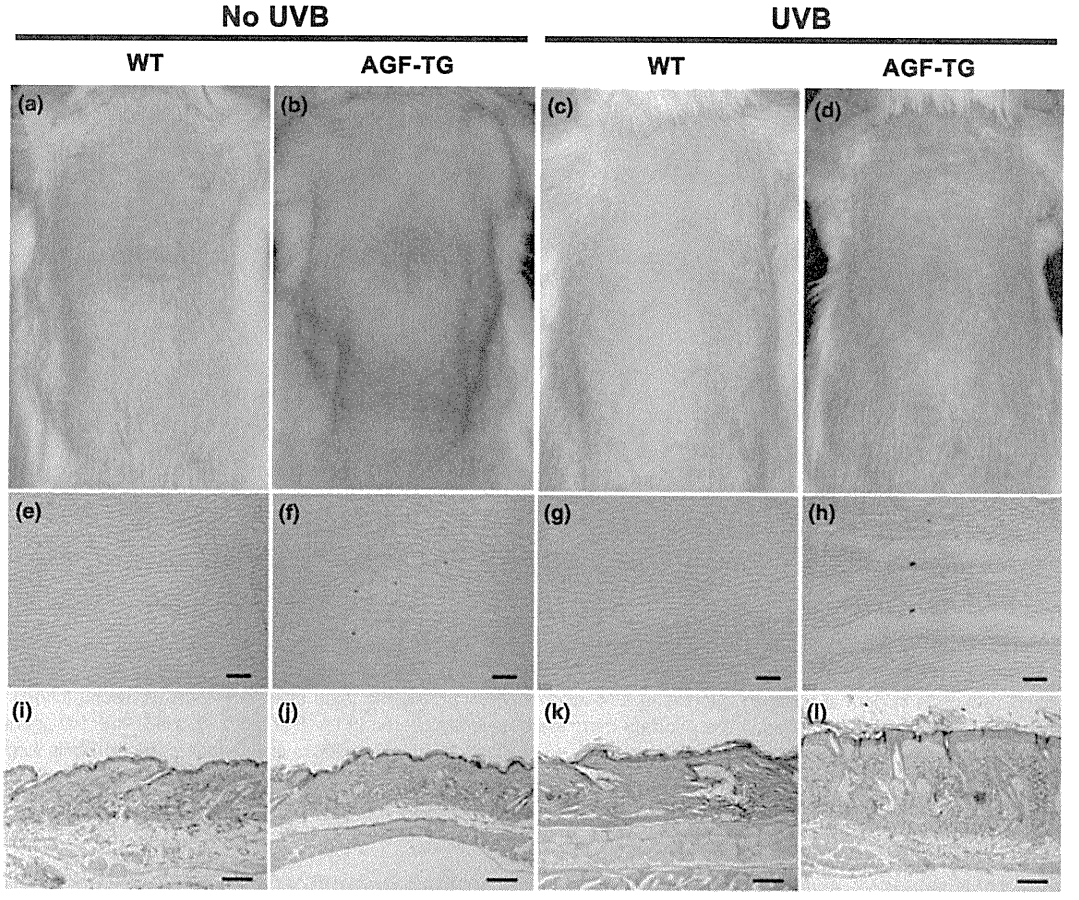

Figure 3. Increased wrinkle formation in Angptl6/AGF-overexpressing mice after long-term ultraviolet (UV)-B irradiation. Dorsal skin of non-irradiated wild-type (WT) and *Angptl6/AGF* transgenic (TG) mice (a,b). After 14 weeks (three times/week) of UV-B irradiation, wild-type mice do not show macroscopic skin alterations (c), whereas *Angptl6/AGF* transgenic mice developed wrinkles and slight erythema (d) (representative images; n = 13/genotype). Skin replicas of wild-type and Angptl6/AGF-overexpressing mice showed no signs of wrinkle formation or texture changes (e,f), nor did those of wild-type mice treated with UV-B (g). Angptl6/AGF-overexpressing mice treated with long-term UV-B irradiation, however, did show wrinkle formation and texture changes (h). (i–l) Hematoxylin–eosin (HE) staining reveals signs of epidermal hyperplasia, edema, inflammatory cell infiltration, and increased vascularization in the papillary dermis in skin of UV-B-irradiated Angptl6/AGF-overexpressing mice (l). The skin of non-irradiated mice of both genotypes (i,j), or of UV-B-irradiated wild-type mice (k) does not show major histological abnormalities. (Scale bars: [e–h] 1 mm, [i–l] 100 μm.)

UV-B. Furthermore, comparable expression levels of VEGF-D were observed in the ears of *Angptl6/AGF* transgenic and wild-type mice under UV-B- or sham-irradiation regimes (Fig. 2j). VEGF-C mRNA levels remained unchanged in either group (data not shown).

To find overall changes of ears in *Angptl6/AGF* transgenic mice and wild-type littermates, we daily measured the ear thickness for 8 days after UV-B irradiation. Seven days after UV-B irradiation, ear thickness was comparable between AGF transgenic mice and wild-type littermates (Fig. 2g). Eight days after UV-B irradiation, the macroscopic appearance of ear skin in *Angptl6/AGF* transgenic mice returned to normal (data not shown). Histologically, ears obtained from *Angptl6/AGF* transgenic mice and wild-type littermates showed comparable cellular morphology 8 days after irradiation based on hematoxylin–eosin staining (Fig. 2k,l). Azan–Mallory staining also indicated little or no degradation of dermal collagen bundles in ears of *Angptl6/AGF* transgenic mice 8 days after irradiation with 9.0×10^{-2} J/cm^2 UV-B (Fig. 2m,n). Together, these results suggest that targeted overexpression of Angptl6/AGF promotes vascular enlargement and subsequent plasma leakage from blood vessels at early stages of UV-B irradiation in murine skin, but that vascular hyperpermeability is not associated with acute photo-induced skin damage.

Angptl6/AGF mediates epidermal hyperplasia in response to chronic UV-B exposure

Overall, we found transient vascular enlargement and reversible ear swelling in *Angptl6/AGF* transgenic mice after a single UV-B exposure but did not observe acute UV-B-induced skin damage or acceleration of the healing process. Therefore, we asked whether targeted Angptl6/AGF overexpression induces skin changes

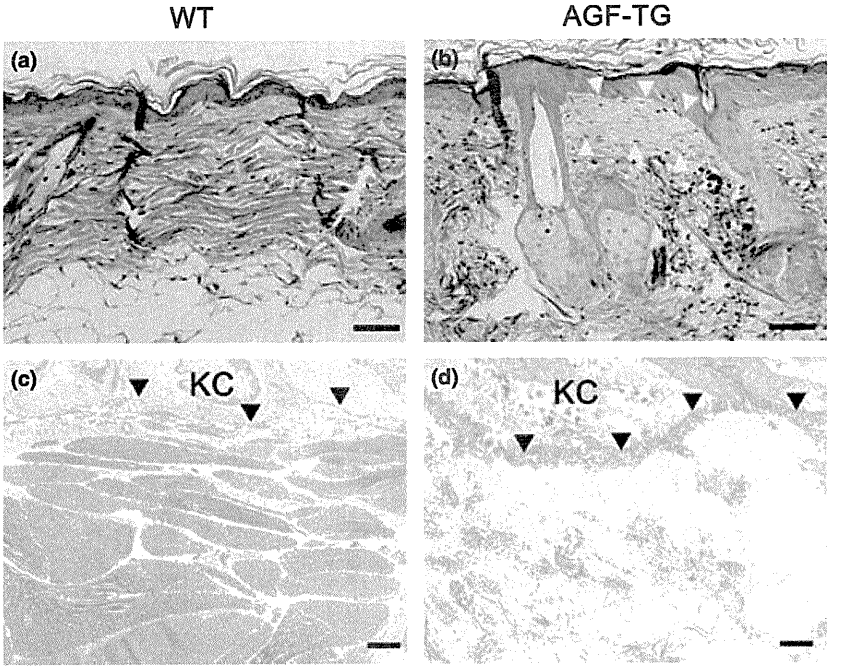

Figure 4. Marked reduction in dermal collagen bundles in *K14–Angptl6/AGF* transgenic mice after long-term ultraviolet (UV)-B. (a,b) Azan–Mallory staining shows that collagen bundles in the papillary dermis are severely altered in UV-B-treated *Angptl6/AGF* transgenic (TG) mice (b, yellows arrows) compared with wild-type (WT) littermates (a). (c,d) Electron micrographs revealed that collagen fibrils and bundles in UV-B-treated AGF transgenic mice were markedly fragmented beneath the dermoepidermal junction (d, arrowheads) compared with wild-type mice (c, arrowheads). (Scale bars: [a,b] 50 μm, [c,d] 2 μm.) KC, keratinocytes.

following chronic UV-B irradiation. *Angptl6/AGF* transgenic mice and wild-type littermates were exposed 3 days a week to a total dose of 8.185 J/cm^2 UV-B for 14 weeks. Wild-type mice showed no skin changes after UV-B irradiation based on both macroscopic appearance (Fig. 3c) and microscopic analysis using skin replicas (Fig. 3g) and appeared comparable in gross appearance to sham-irradiated wild-type mice (Fig. 3a,e). In contrast, the skin of *Angptl6/AGF* transgenic mice exhibited transverse wrinkles after chronic UV-B irradiation (Fig. 3d,h), while sham-irradiated transgenic mice showed little or no wrinkling (Fig. 3b,f). Histologically, the skin of *Angptl6/AGF* transgenic mice showed evidence of epidermal hyperplasia, edema formation and inflammatory cell infiltration in the dermis after chronic UV-B irradiation (Fig. 3l), whereas no such changes were observed in sham-irradiated transgenic mice (Fig. 3j) or in wild-type mice with or without UV-B irradiation (Fig. 3i,k). Azan–Mallory staining showed that the size of collagen bundles was reduced in the upper dermis of *Angptl6/AGF* transgenic mice after chronic UV-B exposure (Fig. 4b), whereas these alterations were not observed in UV-B-irradiated wild-type littermates (Fig. 4a). Moreover, electron microscopic analysis revealed that the regular assembly of collagen was markedly perturbed in the upper dermis of *Angptl6/AGF* transgenic mice after chronic UV-B irradiation (Fig. 4d), whereas the fibrillar collagen network was maintained in the dermis of UV-B-irradiated wild-type mice (Fig. 4c). Together, these results suggest that following chronic UV-B exposure, the skin of *Angptl6/AGF* transgenic mice undergoes alterations leading to wrinkle formation.

Targeted Angptl6/AGF overexpression promotes angiogenesis and lymphatic enlargement in response to chronic UV-B exposure

To determine whether chronic UV-B exposure alters the microvascular network in the skin of *Angptl6/AGF* transgenic mice, we undertook macroscopic and microscopic analyses of blood and lymphatic vessels in the skin. Macroscopic analysis indicated that the skin of transgenic mice was more vascularized after UV-B exposure than that of wild-type littermates either with or without irradiation (Fig. 5a,c,d) or of sham-irradiated transgenic mice (Fig. 5b). Double staining for blood and lymphatic vessels showed that CD31-positive blood vessels were enlarged in the upper dermis of *Angptl6/AGF* transgenic mice after chronic UV-B irradiation (Fig. 5h), whereas few alterations were seen in sham-irradiated transgenic mice or wild-type littermates, either irradiated or not irradiated (Fig. 5e–g). Computer-assisted morphometric analysis of CD31-stained skin sections confirmed that the average number of blood vessels was significantly increased in *Angptl6/AGF* transgenic mice after chronic irradiation (47.23 ± 8.65 blood vessels/mm^2; $P < 0.05$), as compared with sham-irradiated transgenic mice (32.17 ± 3.25 blood vessels/mm^2) or wild-type controls (25.45 ± 3.36 blood vessels/mm^2; Fig. 5j). Furthermore, blood vessels were significantly larger in UV-B-irradiated *Angptl6/AGF* transgenic mice (353.6 ± 41.7 μm^2; $P < 0.05$) than in sham-irradiated transgenic mice (295.6 ± 35.3 μm^2; Fig. 5k). Moreover, we observed a significant increase in the percentage of total tissue area covered by blood vessels in UV-B-irradiated *Angptl6/AGF*

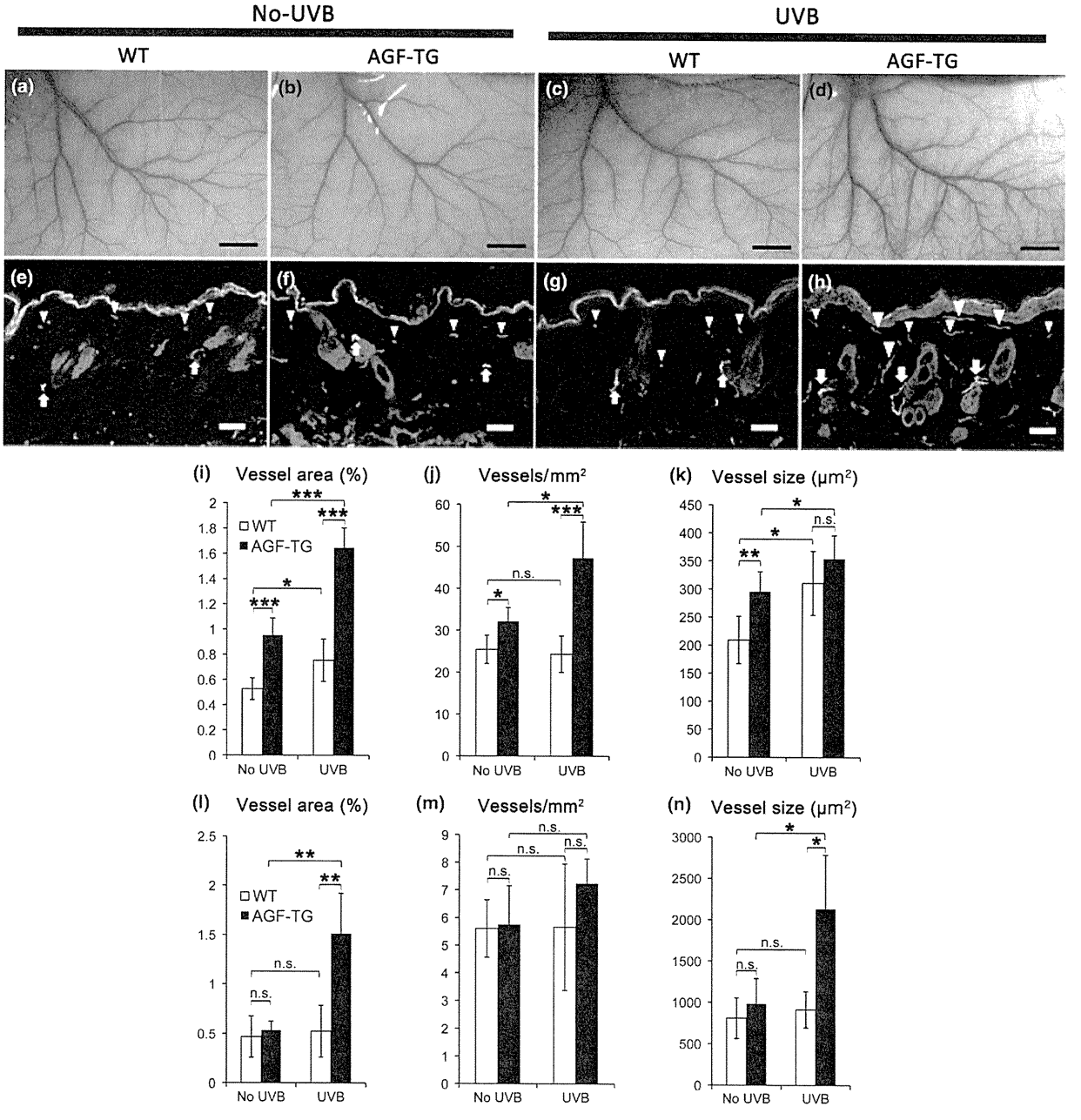

Figure 5. Induction of angiogenesis in *Angptl6/AGF* transgenic (TG) mice after long-term ultraviolet (UV)-B irradiation. (a–d) Increased cutaneous vascularization, with prominent enlargement of blood vessels, is observed after chronic UV-B treatment in the skin of Angptl6/AGF-overexpressing mice (d). Compared with non-irradiated wild-type (WT) littermates (a), no significant changes were observed in wild-type littermates after long-term UV-B irradiation (c) or in Angptl6/AGF-overexpressing mice that did not undergo irradiation (b). (Scale bars: 3 mm.) (e–h) Double immunofluorescence for blood vessels by anti-CD31 antibody (red, arrowheads) and for lymphatic vessels by anti-LYVE-1 antibody (green, arrows) demonstrates prominent vascularization in the dermis of Angptl6/AGF-overexpressing mice after chronic UV-B irradiation (h), whereas few vessels were altered in wild-type littermates that did or did not undergo UV-B irradiation (e,g) and in non-irradiated Angptl6/AGF-overexpressing mice (f). (Scale bars, 50 μm.) (i) Computer-assisted morphometric analysis of CD31-stained skin sections after 14 weeks of UV-B irradiation revealed a significant increase in the relative area occupied by blood vessels (i) and in blood vessel density (j) in *Angptl6/AGF* transgenic mice (■) compared with wild-type littermates (□). (k) Enlargement of blood vessels detected by CD31 staining is prominent in UV-B-treated *Angptl6/AGF* transgenic mice. Skin sections after 14 weeks of UV-B irradiation show a significant increase in the relative area occupied by lymphatic vessels (l) and in average vessel size (n) in *Angptl6/AGF* transgenic mice (■) compared with wild-type mice. In contrast, no significant differences were observed in the vessel density (m) between non-irradiated and irradiated skin of AGF transgenic mice (■) and wild-type littermates (□). Data are expressed as mean ± standard deviation ($n = 5$). ***$P < 0.001$; **$P < 0.01$; *$P < 0.05$.

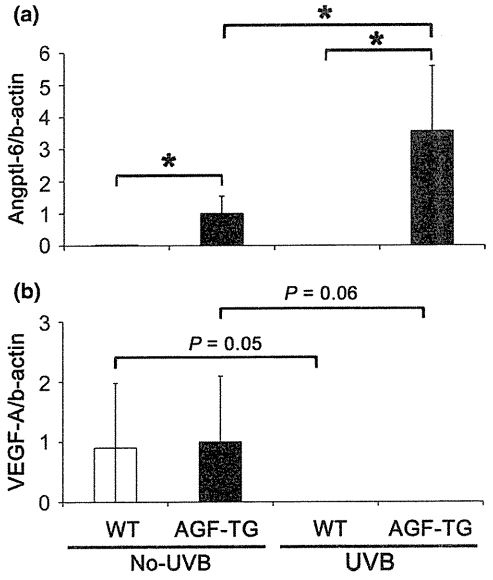

Figure 6. Chronic ultraviolet (UV)-B exposure promotes increased levels of Angptl6/AGF mRNA and decreased levels of vascular endothelial growth factor (VEGF)-A mRNA. (a) Angptl6/AGF mRNA levels were significantly increased in the skin of UV-B-exposed transgenic (TG) mice compared with wild-type littermates. (b) In contrast, VEGF-A mRNA expression in the skin was undetectable after UV-B irradiation of either wild-type or *Angptl6/AGF* transgenic mice.

transgenic mice (1.65 ± 0.16%) compared with controls (0.75 ± 0.17%; $P < 0.001$) (Fig. 5i). Lymphatic-specific staining with LYVE-1 revealed marked enlargement of dermal lymphatic vessels in UV-B-irradiated skin of *Angptl6/AGF* transgenic mice (Fig. 5h) compared with sham-irradiated transgenic mice (Fig. 5f) or irradiated or non-irradiated wild-type mice (Fig. 5e,g). Computer-assisted morphometric analysis showed that the size of dermal lymphatic vessels is significantly increased by twofold ($P < 0.05$) in *Angptl6/AGF* transgenic mice after chronic UV-B irradiation (2129.2 ± 654.1 μm^2; $P < 0.05$) compared with non-irradiated transgenic mice (981.5 ± 305.4 μm^2), or wild-type controls with or without UV-B irradiation (911.2 ± 219.3 μm^2 or 807.7 ± 242.6 μm^2, respectively; Fig. 5n). The percentage of total tissue area covered by lymphatic vessels of *Angptl6/AGF*-overexpressing skin was significantly increased after chronic UV-B-irradiation (1.51 ± 0.41%; $P < 0.001$) compared with sham-irradiated *Angptl6/AGF* transgenic mice (0.53 ± 0.09%) or wild-type controls with or without UV-B irradiation (0.52 ± 0.26% or 0.47 ± 0.21%, respectively; Fig. 5l). However, the average density of dermal lymphatics in both genotypes with or without chronic UV-B exposure was comparable (Fig. 5m). Importantly, increased levels of ectopic *Angptl6/AGF* mRNA were observed in UV-B-exposed skin of *Angptl6/AGF* transgenic mice as compared with sham-irradiated skin of transgenic mice (Fig. 6). No changes in VEGF-A mRNA levels were observed in UV-B-exposed skin of either *Angptl6/AGF* transgenic or wild-type mice (Fig. 6). Together, these results suggest that overexpression of *Angptl6/AGF* in mouse skin promotes prominent angiogenesis and subsequent enlargement of lymphatic vessels.

DISCUSSION

In this study, we subjected *Angptl6/AGF* transgenic mice to UV-B exposure, a major risk for cutaneous damage, to test the hypothesis that Angptl6/AGF might reduce acute and/or chronic skin damage by accelerating tissue repair. Interestingly, however, our results indicate that chronic UV-B activates the K14 promoter driving the Angptl6/AGF transgene, resulting in photo-induced skin alterations at a subthreshold UV-B dose that induced little or no skin changes in wild-type littermates.

Recent studies indicate that UV-B potently induces an angiogenic switch, namely, upregulates pro-angiogenic mediators and downregulates anti-angiogenic ones, leading to a pathological pro-angiogenic condition in the skin.[9] In support of this concept, targeted VEGF-A overexpression in mouse skin was shown to promote vascular enlargement and subsequent vascular leakage in response to a single UV-B exposure.[9] In addition, VEGF-A transgenic mice showed increased inflammatory cell infiltration in the dermis and epidermal hyperplasia at subthreshold UV-B doses, features typical of acute UV-B-induced skin damage.[9] In contrast, in the present study, targeted Angptl6/AGF overexpression in mouse skin promoted little or no epidermal hyperplasia in response to a single UV-B exposure, although marked enlargement of cutaneous blood vessels was observed. In fact, Angptl6/AGF has been shown to increase the vascular network of capillary-sized blood vessels in a physiological pattern,[17] whereas VEGF-A induces formation of tortuous, capillary-sized blood vessels in transgenic mice, leading to promotion of leukocyte trafficking and rolling.[20] Therefore, physiological induction of AGF by a single UV-B exposure may prevent enhanced vascular leakage, which would initiate cutaneous inflammation and subsequent epidermal hyperplasia.

In contrast to a single UV-B exposure, chronic UV-B exposure over 14 weeks was accompanied by prominent skin alterations, including epidermal hyperplasia, in *Angptl6/AGF* transgenic mice as compared with wild-type littermates. Overproduction of AGF over a long period may underlie the development of wrinkles seen in response to chronic UV-B irradiation. In fact, in this study, a total dose of 8.156 J/cm^2 UV-B was required to promote development of macroscopic wrinkles in *K14–Angptl6/AGF* transgenic mice, whereas a total dose of 0.72 J/cm^2 UV-B was sufficient to induce chronic photo-induced skin damage in irradiated *K14–VEGF-A* transgenic mice.[9] Interestingly, no induction of VEGF-A mRNA was found in *Angptl6/AGF* transgenic mice which were exposed to the long-term UV-B irradiation in the skin, whereas *Angptl6/AGF* mRNA levels were significantly increased in those mice. Therefore, these findings suggest that long-term UV-B irradiation activates the K14 promoter driving the *Angptl6/AGF* transgene, and that the ectopic overexpression of AGF actively promotes the development of chronic photo-induced skin alterations in an independent manner.

Dermal lymphatic vessels were markedly enlarged in *Angptl6/AGF* transgenic mice after chronic UV-B exposure. In contrast, little or no lymphatic vessel alteration was seen in sham-irradiated *Angptl6/AGF* transgenic mice compared with wild-type littermates. Does experimental induction of Angptl6/AGF by chronic UV-B exposure mediate dilation of lymphatic vessels? The skin of

UV-B-exposed *Angptl6/AGF* transgenic mice exhibits signs of enhanced angiogenesis reflected by an increased number of blood vessels compared to sham-irradiated mice. In contrast, the density of lymphatic vessels was comparable between chronic UV-B- and sham-irradiated *Angptl6/AGF* mice, suggesting that Angptl6/AGF does not induce lymphangiogenesis as it does angiogenesis. However, increased blood flow can induce uptake and subsequent transport of fluids by dermal lymphatic vessels, likely promoting significant enlargement of the lymphatic vasculature. Importantly, chronic UV-B exposure markedly upregulated Angptl6/AGF mRNA levels, whereas no upregulation of VEGF-A mRNA levels was observed in this model. VEGF-A, but not VEGF-C or VEGF-D, was previously shown to be upregulated in *hairless* mice in response to chronic UV-B exposure, an effect accompanied by enlargement and impairment of lymphatic vessels.[14] Furthermore, functional inactivation of VEGF-A inhibits enlargement of lymphatic vessels after a single UV-B exposure, suggesting that VEGF-A is responsible for both vascular hyperpermeability and reduced lymphatic drainage in response to UV-B exposure.[14] Therefore, angiogenesis and increased blood flow likely promote enlargement of lymphatic vessels and alter their function in chronic UV-B-induced skin damage. Accordingly, Angptl6/AGF has been recently shown to enhance blood flow in a mouse hind-limb ischemia model.[21] In addition, epidermal overexpression of Angptl2 promotes marked enlargement of lymphatic and blood vessels in the skin. Moreover, sufficient lymphatic flow is required to minimize tissue edema and subsequent inflammation in response to UV-B irradiation.[22] Therefore, future studies should address whether UV-B irradiation alters lymphatic flow and/or function in Angptl transgenic mice, and whether metastasis associated with UV-B-induced carcinogenesis is correlated with changes in lymphatic vessel function.

ACKNOWLEDGMENTS

The authors thank Mika Ikeda, Eriko Tan and Teruko Tsuda for technical assistance. The Japanese Society for Investigative Dermatology Fellowship SHISEIDO Award 2008 (to S. H.), and a Grant-in-Aid for Scientific Research from the Ministry of Education, Culture, Sports, Science, and Technology of Japan (to Y. N.).

REFERENCES

1 Folkman J. Tumor angiogenesis: therapeutic implications. *N Eng J Med* 1971; **285**: 1182–1186.
2 Dvorak HF, Brown LF, Detmar M, Dvorak AM. Vascular permeability factor/vascular endothelial growth factor, microvascular hyperpermeability, and angiogenesis. *Am J Pathol* 1995; **146**: 1029–1239.
3 Kligman LH. Symposium on models for the study of human photoaging: American Society for Photobiology. *Photochem Photobiol* 1989; **50**: 903–905.
4 Yano K, Oura H, Detmar M. Targeted overexpression of the angiogenesis inhibitor thrombospondin-1 in the epidermis of transgenic mice prevents ultraviolet-B-induced angiogenesis and cutaneous photo-damage. *J Invest Dermatol* 2002; **118**: 800–805.
5 Yano K, Kadoya K, Kajiya K, Hong YK, Detmar M. Ultraviolet B irradiation of human skin induces an angiogenic switch that is mediated by upregulation of vascular endothelial growth factor and by downregulation of thrombospondin-1. *Br J Dermatol* 2005 (Jan); **152** (1): 115–121.
6 Kramer M, Sachsenmaier C, Herrlich P, Rahmsdorf HJ. UV irradiation-induced interleukin-1 and basic fibroblast growth factor synthesis and release mediate part of the UV response. *J Biol Chem* 1993; **268**: 6734–6741.
7 Strickland I, Rhodes LE, Flanagan BF, Friedmann PS. TNF-alpha and IL-8 are upregulated in the epidermis of normal human skin after UVB exposure: correlation with neutrophil accumulation and E-selectin expression. *J Invest Dermatol* 1997; **108**: 763–768.
8 Bielenberg DR, Bucana CD, Sanchez R, Donawho CK, Kripke ML, Fidler IJ. Molecular regulation of UVB-induced cutaneous angiogenesis. *J Invest Dermatol* 1998; **111**: 864–872.
9 Hirakawa S, Fujii S, Kajiya K, Yano K, Detmar M. Vascular endothelial growth factor promotes sensitivity to ultraviolet B-induced cutaneous photodamage. *Blood* 2005; **105**: 2392–2399.
10 Oike Y, Ito Y, Maekawa H *et al.* Angiopoietin-related growth factor (AGF) promotes angiogenesis. *Blood* 2004; **103**: 3760–3765.
11 Oike Y, Akao M, Yasunaga K *et al.* Angiopoietin-related growth factor antagonizes obesity and insulin resistance. *Nat Med* 2005; **11**: 400–408.
12 Hato T, Tabata M, Oike Y. The role of angiopoietin-like proteins in angiogenesis and metabolism. *Trends Cardiovasc Med* 2008 (Jan); **18** (1): 6–14.
13 Oike Y, Yasunaga K, Ito Y *et al.* Angiopoietin-related growth factor (AGF) promotes epidermal proliferation, remodeling, and regeneration. *Proc Natl Acad Sci USA* 2003; **100**: 9494–9499.
14 Kajiya K, Hirakawa S, Detmar M. Vascular endothelial growth factor-A mediates ultraviolet B-induced impairment of lymphatic vessel function. *Am J Pathol* 2006; **169**: 1496–1503.
15 Hirakawa S, Detmar M. New insights into the biology and pathology of the cutaneous lymphatic system. *J Dermatol Sci* 2004 (Jun); **35** (1): 1–8.
16 Kajiya K, Sawane M, Huggenberger R, Detmar M. Activation of the VEGFR-3 pathway by VEGF-C attenuates UVB-induced edema formation and skin inflammation by promoting lymphangiogenesis. *J Invest Dermatol* 2009; **129**: 1292–1298.
17 Tabata M, Kadomatsu T, Fukuhara S *et al.* Angiopoietin-like protein 2 promotes chronic adipose tissue inflammation and obesity-related systemic insulin resistance. *Cell Metab* 2009; **10**: 178–188.
18 Hirakawa S, Kodama S, Kunstfeld R, Kajiya K, Brown LF, Detmar M. VEGF-A induces tumor and sentinel lymph node lymphangiogenesis and promotes lymphatic metastasis. *J Exp Med* 2005; **201**: 1089–1099.
19 Hirakawa S, Detmar M, Kerjaschki D *et al.* Nodal lymphangiogenesis and metastasis: role of tumor-induced lymphatic vessel activation in extramammary Paget's disease. *Am J Pathol* 2009; **175**: 2235–2248.
20 Detmar M, Brown LF, Schön MP *et al.* Increased microvascular density and enhanced leukocyte rolling and adhesion in the skin of VEGF transgenic mice. *J Invest Dermatol* 1998; **111**: 1–6.
21 Urano T, Ito Y, Akao M *et al.* Angiopoietin-related growth factor enhances blood flow via activation of the ERK1/2-eNOS-NO pathway in a mouse hind-limb ischemia model. *Arterioscler Thromb Vasc Biol* 2008; **28**: 827–834.
22 Kajiya K, Detmar M. An important role of lymphatic vessels in the control of UVB-induced edema formation and inflammation. *J Invest Dermatol* 2006; **126**: 919–921.

EphrinA/EphA signal facilitates insulin-like growth factor-I–induced myogenic differentiation through suppression of the Ras/extracellular signal–regulated kinase 1/2 cascade in myoblast cell lines

Masayoshi Minami[a], Tatsuya Koyama[a,b], Yuki Wakayama[a], Shigetomo Fukuhara[a], and Naoki Mochizuki[a]

[a]Department of Cell Biology, National Cerebral and Cardiovascular Center Research Institute, Osaka 565-8565, Japan; [b]Division of Cardiology, Department of Internal Medicine, Jikei University School of Medicine, Tokyo 105-8461, Japan

ABSTRACT **Insulin-like growth factor-I (IGF-I) activates not only the phosphatidylinositol 3-kinase (PI3K)–AKT cascade that is essential for myogenic differentiation but also the extracellular signal–regulated kinase (ERK) 1/2 cascade that inhibits myogenesis. We hypothesized that there must be a signal that inhibits ERK1/2 upon cell–cell contact required for skeletal myogenesis. Cell–cell contact–induced engagement of ephrin ligands and Eph receptors leads to downregulation of the Ras-ERK1/2 pathway through p120 Ras GTPase-activating protein (p120RasGAP). We therefore investigated the significance of the ephrin/Eph signal in IGF-I–induced myogenesis. EphrinA1-Fc suppressed IGF-I–induced activation of Ras and ERK1/2, but not that of AKT, in C2C12 myoblasts, whereas ephrinB1-Fc affected neither ERK1/2 nor AKT activated by IGF-I. IGF-I–dependent myogenic differentiation of C2C12 myoblasts was potentiated by ephrinA1-Fc. In p120RasGAP-depleted cells, ephrinA1-Fc failed to suppress the Ras-ERK1/2 cascade by IGF-I and to promote IGF-I–mediated myogenesis. EphrinA1-Fc did not promote IGF-I–dependent myogenesis when the ERK1/2 was constitutively activated. Furthermore, a dominant-negative EphA receptor blunted IGF-I–induced myogenesis in C2C12 and L6 myoblasts. However, the inhibition of IGF-I–mediated myogenesis by down-regulation of ephrinA/EphA signal was canceled by inactivation of the ERK1/2 pathway. Collectively, these findings demonstrate that the ephrinA/EphA signal facilitates IGF-I–induced myogenesis by suppressing the Ras-ERK1/2 cascade through p120RasGAP in myoblast cell lines.**

Monitoring Editor
Richard K. Assoian
University of Pennsylvania

Received: Mar 7, 2011
Revised: Jul 14, 2011
Accepted: Jul 21, 2011

This article was published online ahead of print in MBoC in Press (http://www.molbiolcell.org/cgi/doi/10.1091/mbc.E11-03-0183) on July 27, 2011.

Address correspondence to: Shigetomo Fukuhara (fuku@ri.ncvc.go.jp).

Abbreviations used: Ang1, angiopoietin-1; β-gal, β-galactosidase; bFGF, basic fibroblast growth factor; caMEK1, constitutively active form of MEK1; COMP, cartilage oligomeric matrix protein; EphA2Δcyto, EphA2 mutant that lacks the cytoplasmic region; ERK, extracellular signal–regulated kinase; FBS, fetal bovine serum; Ig, immunoglobulin; IGF, insulin-like growth factor; MAPK, mitogen-activated protein kinase; MEK1/2, MAPK/ERK kinase1/2; MHC, myosin heavy chain; p120RasGAP, p120 Ras GTPase-activating protein; PI3K, phosphatidylinositol 3-kinase; RTK, receptor tyrosine kinase; siRNA, small interfering RNA.

INTRODUCTION

Skeletal myogenesis is a complex process that begins with the commitment of multipotent mesodermal precursor cells to the muscle fate (Andres and Walsh, 1996; Taylor, 2002). These committed cells—the myoblasts—subsequently withdraw from the cell cycle, differentiate, and fuse into multinucleated myotubes. In culture, most skeletal muscle cell lines proliferate under high serum conditions, whereas the cells placed under low serum conditions spontaneously undergo differentiation into myotubes (Florini *et al.*, 1991; Ewton *et al.*, 1994; Bach *et al.*, 1995).

Differentiation of skeletal muscle cells is positively and negatively regulated by two major intracellular signaling pathways, namely the phosphatidylinositol 3-kinase (PI3K)–AKT cascade and the extracellular signal–regulated kinase (ERK) 1/2 cascade (Kaliman *et al.*, 1996,

1998; Bennett and Tonks, 1997; Coolican *et al.*, 1997; Tortorella *et al.*, 2001; de Alvaro *et al.*, 2005; Koyama *et al.*, 2008). The latter involves Ras, Raf, mitogen-activated protein kinase (MAPK)/ERK kinase1/2 (MEK1/2), and ERK1/2. Activation of ERK1/2 cascade evoked by mitogens induces proliferation of cultured skeletal muscle cells but prevents their differentiation (Bennett and Tonks, 1997; Coolican *et al.*, 1997; Tortorella *et al.*, 2001; de Alvaro *et al.*, 2005; Koyama *et al.*, 2008). Among various growth factors, the insulin-like growth factors (IGFs), including IGF-I and IGF-II, have been reported to be quite singular, in that they stimulate both proliferation and differentiation of muscle cells in culture (Florini *et al.*, 1991, 1996; Coolican *et al.*, 1997; Kaliman *et al.*, 1998; Koyama *et al.*, 2008; Clemmons, 2009).

IGF-I receptor, which belongs to receptor tyrosine kinase (RTK) family, activates the PI3K–AKT signaling cascade in response to IGFs, thereby promoting differentiation of skeletal muscle cells (Florini *et al.*, 1996; Coolican *et al.*, 1997; Kaliman *et al.*, 1998; White, 2003). The importance of the IGF/IGF-I receptor signal in muscle development is also illustrated by the poor muscle development and dystrophic phenotype of IGF-I receptor–deficient mice (Liu *et al.*, 1993). However, the IGF/IGF-I receptor signal also induces activation of ERK1/2 through Grb2-associated binder 1–SHP2 signaling pathways in C2C12 cells, which counteracts PI3K/AKT signal-mediated myogenic differentiation (Coolican *et al.*, 1997; Koyama *et al.*, 2008). Thus the differentiation of myoblasts into myotubes is determined by the balance between the positive and negative signals mediated through PI3K–AKT and ERK1/2 cascades, respectively.

Myoblast differentiation is regulated not only by the signaling pathways induced by soluble myogenic growth factors but also by those initiated by cell–cell contacts (Krauss, 2010; Pavlath, 2010). Cell–cell adhesions are constituted by cadherin and other junctional molecules. Among them, N-cadherin (also known as cadherin-2) is expressed throughout skeletal myogenesis and was shown to be involved in myogenic differentiation in myoblast cell lines (Charrasse *et al.*, 2002; Gavard *et al.*, 2004; Lovett *et al.*, 2006; Krauss, 2010). N-cadherin associates in *cis* with Cdo, a cell surface receptor of the immunoglobulin (Ig) superfamily in C2C12 myoblasts (Lu and Krauss, 2010). On N-cadherin ligation, the Cdo intracellular region binds to Bnip-2, a scaffold protein for Cdc42 small GTPase, and to JLP, a scaffold protein for the p38α/β MAPK, which results in Cdc42-dependent activation of p38α/β (Takaesu *et al.*, 2006; Kang *et al.*, 2008). In contrast to ERK1/2 MAPK, the p38α/β pathway promotes skeletal myogenesis by inducing the expression of muscle-specific genes in myoblast cell lines and primary myoblasts (Guasconi and Puri, 2009). Thus, upon cell–cell contact formation, the N-cadherin/Cdo complex promotes myogenic differentiation through activation of the p38α/β pathway. N-cadherin engagement also induces activation of RhoA, leading to serum response factor–dependent expression of muscle-specific genes in skeletal muscle cell lines (Carnac *et al.*, 1998). It has also been suggested that M-cadherin, another member of the classic cadherin family, regulates myoblast fusion through Trio guanine nucleotide exchange factor–dependent activation of Rac1 in C2C12 myoblasts (Charrasse *et al.*, 2007). In addition to cadherins, Ig superfamily members such as neogenin and neural cell adhesion molecule also regulate myogenic differentiation of cultured myoblasts in a cell–cell contact–dependent manner (Kang *et al.*, 2004; Krauss, 2010). These results reveal the importance of the signaling pathways mediated by cell–cell contacts for myoblast differentiation.

Eph receptors and their ligands—ephrins—constitute the largest subfamily of RTKs, and have been implicated in diverse physiological and pathophysiological functions, such as neural development, angiogenesis, and tumorigenesis (Pasquale, 2005, 2008). The Eph receptors are divided into two classes, EphA and EphB, based on their ability to bind the ligands ephrinA and ephrinB, respectively. Unlike other RTK ligands, both ephrinA and ephrinB are membrane-bound proteins (Pasquale, 2005, 2008). EphrinAs anchor to the plasma membrane via a glycosylphosphatidylinositol moiety, whereas ephrinBs contain a transmembrane domain. Thus ephrin/Eph signaling is initiated by the formation of cell–cell contacts (Pasquale, 2010). On ephrin binding, Eph receptors undergo autophosphorylation at tyrosine residues in the cytoplasmic domain, which then triggers downstream signaling cascades through interaction with several signaling molecules, including p120 Ras GTPase-activating protein (p120RasGAP) (Pasquale, 2010). It has been shown that the ephrin/Eph signal negatively regulates the Ras-ERK1/2 cascade through inhibition of Ras by p120RasGAP in various types of cell lines (Elowe *et al.*, 2001; Miao *et al.*, 2001; Tong *et al.*, 2003; Parri *et al.*, 2005; Pasquale, 2010). The evidence that the Eph/ephrin signal depends on cell–cell contacts and its ability to down-regulate the Ras-ERK1/2 cascade prompted us to test our hypothesis that the ephrin/Eph signal promotes myogenic differentiation by reducing the myogenic inhibitory signal mediated by the Ras-ERK1/2 cascade. In this study, we found that the cell–cell contact–dependent ephrinA/EphA signal down-regulates the IGF-I–induced ERK1/2 pathway through p120RasGAP in myoblast cell lines, thereby accelerating myogenic differentiation.

RESULTS

EphrinA/EphA signal represses IGF-I–induced activation of ERK1/2, but not AKT, through p120RasGAP in mouse C2C12 and rat L6 myoblasts

To investigate whether the ephrin/Eph signal downregulates the Ras-ERK1/2 cascade in myoblasts, we examined the effect of ephrinA1-Fc or ephrinB1-Fc on IGF-I–induced activation of ERK1/2 and AKT in myoblast cell lines. IGF-I induced activation of both ERK1/2 and AKT in sparse cultures of mouse C2C12 and rat L6 cells (Figure 1 and Supplemental Figure S1, A and B). EphrinA1-Fc, but not Fc, dramatically suppressed IGF-I–induced activation of ERK1/2 (Figure 1 and Supplemental Figure S1, A and B). In clear contrast, IGF-I–induced activation of AKT was unaffected by ephrinA1-Fc (Figure 1 and Supplemental Figure S1, A and B). EphrinB1-Fc did not affect IGF-I–induced activation of ERK1/2 and AKT in C2C12 cells (Supplemental Figure S1C). To confirm that ephrinB1-Fc used in this experiment is functional, we also examined the effect of ephrinB1-Fc on activation of ERK1/2 by cartilage oligomeric matrix protein (COMP)–angiopoietin-1 (Ang1), a potent Ang1 variant, in human umbilical vein endothelial cells, since it was reported that the ephrinB/EphB signal suppresses Ang1-induced activation of ERK1/2 in endothelial cells (Kim *et al.*, 2002). COMP-Ang1–induced activation of ERK1/2 was clearly attenuated by the treatment with ephrinB1-Fc (Supplemental Figure S1D). These results indicate that the ephrinA/EphA signal, but not the ephrinB/EphB signal, downregulates the IGF-I–induced ERK1/2 cascade without affecting the AKT activation by IGF-I in C2C12 and L6 myoblasts.

It is known that p120RasGAP is recruited to the ephrinA-stimulated EphA receptors, leading to down-regulation of the Ras–ERK1/2 pathway (Pasquale, 2010). Thus we next investigated whether the ephrinA/EphA signal down-regulates the IGF-I–induced ERK1/2 cascade by decreasing Ras activity through p120RasGAP. IGF-I induced activation of Ras in C2C12 myoblasts (Figure 2A). IGF-1–induced Ras activation was suppressed by ephrinA1-Fc (Figure 2A). However, ephrinA1-Fc failed to suppress the IGF-I–induced Ras activation when p120RasGAP was depleted by small interfering RNAs

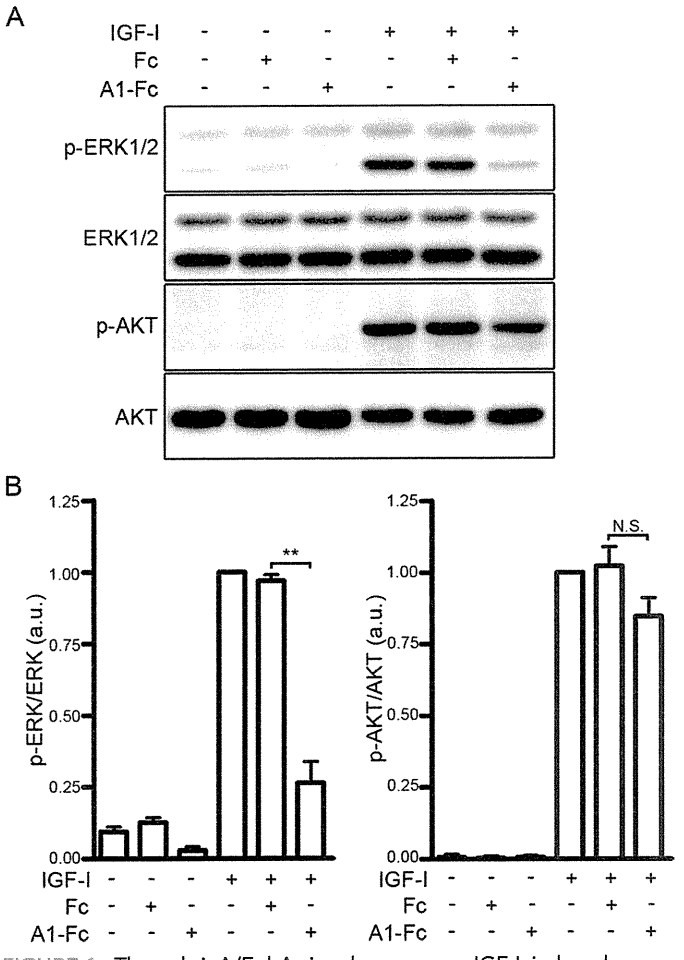

FIGURE 1: The ephrinA/EphA signal suppresses IGF-I–induced activation of ERK1/2 in C2C12 myoblasts. (A) Serum-starved C2C12 myoblasts were stimulated for 10 min with or without 10 nM IGF-I in the presence or absence of 1.7 nM Fc (Fc) or ephrinA1-Fc (A1-Fc) as indicated at the top. Cell lysates were subjected to Western blot analysis with anti–phospho-ERK1/2 (p-ERK1/2), anti-ERK1/2 (ERK1/2), anti–phospho-AKT (p-AKT), and anti-AKT (AKT) antibodies as indicated at the left. (B) Phosphorylation levels of ERK1/2 (left) and AKT (right) observed in A were quantified and represented by the ratio of phospho-ERK1/2 or phospho-AKT to total ERK1/2 or total AKT, respectively. The value for each group is expressed relative to the ratio observed in the cells stimulated with IGF-I in the absence of Fc and ephrinA1-Fc and shown as means ± SD of three independent experiments. **$p < 0.01$, significant difference between two groups. N.S., no significance between two groups. a.u., arbitrary unit(s).

(siRNAs; Figure 2A). Consistently, depletion of p120RasGAP by siRNA blunted the inhibitory effect of ephrinA1-Fc on IGF-I–induced activation of ERK1/2, although it had no effect on IGF-I–induced activation of ERK1/2 and AKT (Figure 2, B and C). Collectively, these findings indicate that the ephrinA/EphA signal downregulates the IGF-I–evoked Ras–ERK1/2 cascade through p120RasGAP in C2C12 myoblasts.

EphrinA/EphA signal enhances IGF-I–induced myogenic differentiation

Myogenic differentiation is negatively and positively regulated by the ERK1/2 and AKT cascades, respectively (Kaliman *et al.*, 1996, 1998; Bennett and Tonks, 1997; Coolican *et al.*, 1997; Tortorella *et al.*, 2001; de Alvaro *et al.*, 2005; Koyama *et al.*, 2008). Because the ephrinA/EphA signal downregulates the ERK1/2 cascade without affecting the AKT pathway in myoblast cell lines, we hypothesized that myogenic differentiation might be enhanced by the ephrinA/EphA signal. To address this possibility, confluent C2C12 myoblasts were differentiated into myotubes by being incubated in DMEM containing 1% fetal bovine serum (FBS) and 10 nM IGF-I in the presence of either Fc or ephrinA1-Fc. To evaluate myogenic differentiation, the expression of muscle-specific myosin heavy chain (MHC) protein was examined by immunocytochemical and Western blot analyses. On the third day after induction of myogenic differentiation, formation of MHC-positive myotubes was greater in the cells differentiated in the presence of ephrinA1-Fc than in those in the presence of Fc (control; Figure 3, A and B). Consistently, expression of MHC protein was 2.4 and 1.6 times higher in the ephrinA1-Fc–treated cells than in those treated with Fc on the second and third days after induction of differentiation, respectively (Figure 3, C and D). Similarly, myogenic differentiation of C2C12 cells induced by low concentrations of IGF-I was also potentiated by the treatment with ephrinA1-Fc (Supplemental Figure S2). These results indicate that activation of the ephrinA/EphA signal results in enhancement of IGF-I–dependent myogenic differentiation in C2C12 cells.

EphrinA/EphA signal promotes IGF-I–induced myogenic differentiation by suppressing the Ras–ERK1/2 cascade through p120RasGAP

To investigate whether the ephrinA/EphA signal promotes IGF-I–dependent myogenic differentiation by suppressing the Ras–ERK1/2 pathway through p120RasGAP, we examined the effect of p120RasGAP depletion on the enhancement of IGF-I–induced myogenic differentiation by the ephrinA/EphA signal. C2C12 myoblasts transfected with either control siRNA or two independent siRNAs targeting p120RasGAP were differentiated in the media containing both IGF-I and ephrinA1-Fc for 2 d. Myogenic differentiation of C2C12 cells was significantly suppressed in the p120RasGAP-depleted cells compared to the cells transfected with control siRNA, as assessed by immunocytochemical analysis with anti-MHC antibody (Figure 4, A and B). Consistently, the expression of MHC was decreased by the depletion of p120RasGAP (Figure 4, C and D). These findings show that the ephrinA/EphA signal implicates p120RasGAP in the enhancement of the IGF-I–induced myogenic differentiation of C2C12 cells.

To further clarify whether the ephrinA/EphA signal promotes IGF-I–dependent myogenic differentiation through inactivation of ERK1/2 pathway, we examined the effect of adenovirus-mediated overexpression of a constitutively active mutant of MEK1 (caMEK1). As expected, overexpression of caMEK1 in C2C12 cells resulted in constitutive activation of ERK1/2 (Figure 5A). Inactivation of ERK1/2 in response to IGF-I by ephrinA1-Fc was canceled in the cells expressing caMEK1, although overexpression of caMEK1 did not affect IGF-I–induced AKT activation in the presence or absence of ephrinA1-Fc (Figure 5A). In the C2C12 myoblasts expressing caMEK1, IGF-I failed to induce formation of MHC-positive myotubes even in the presence of ephrinA1-Fc (Figure 5, B and C). Consistently, IGF-I–induced expression of MHC was prevented by overexpression of caMEK1 irrespective of the presence or absence of ephrinA1-Fc (Figure 5, D and E). Collectively, these findings indicate that the ephrinA/EphA signal potentiates IGF-I–induced myogenic differentiation of C2C12 cells through p120RasGAP-mediated down-regulation of the Ras–ERK1/2 cascade.

EphA2 receptor that lacks the cytoplasmic domain acts as a dominant-negative mutant for EphA family members

We further investigated whether the ephrinA/EphA signal is required for IGF-I–dependent myogenic differentiation. Because reverse

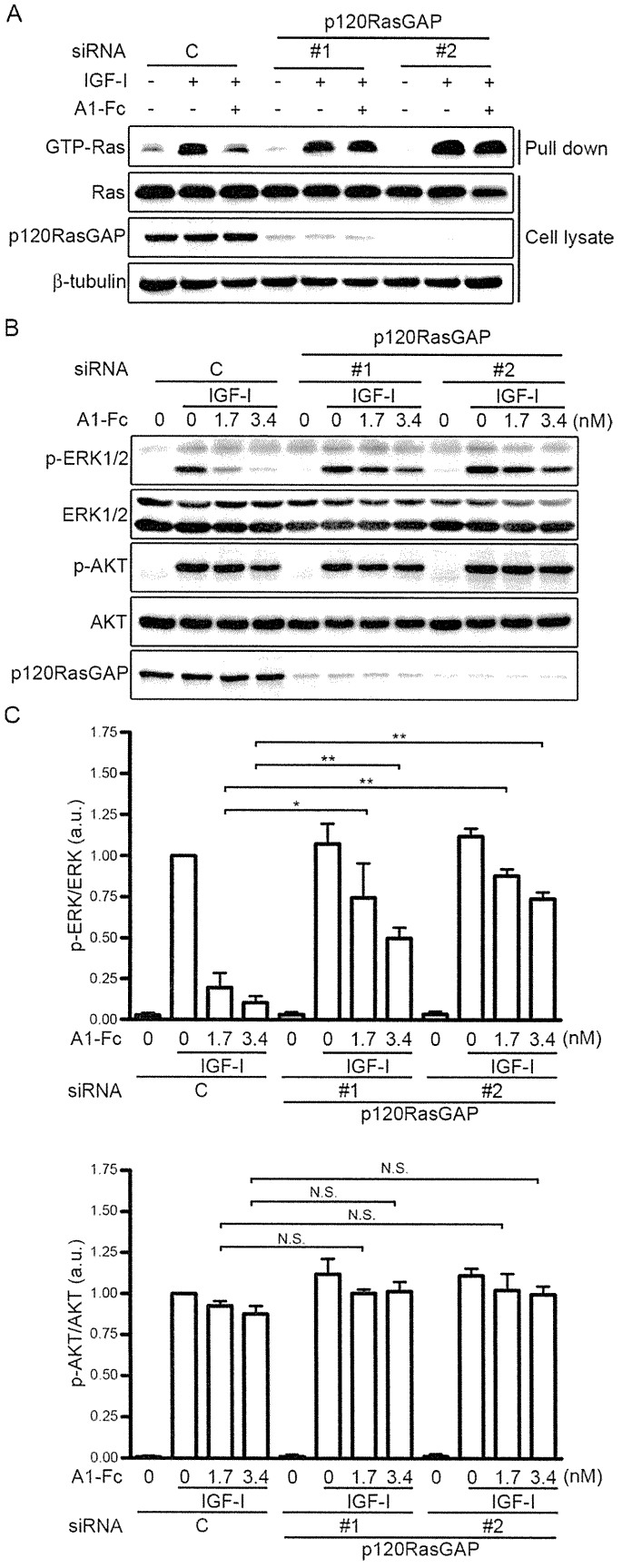

FIGURE 2: The ephrinA/EphA signal suppresses the IGF-I–induced Ras–ERK1/2 pathway through p120RasGAP. (A) Serum-starved C2C12 myoblasts transfected with either control siRNA (C) or two independent siRNAs targeting p120RasGAP (1 and 2) were stimulated for 5 min with or without 10 nM IGF-1 in the absence (–) or presence (+) of 1.7 nM ephrinA1-Fc (A1-Fc) as indicated at the top. GTP-bound Ras was collected as described in *Materials and Methods* and subjected to Western blot analysis with anti-Ras antibody (GTP-Ras). Aliquots of cell lysates were also subjected to Western blot analysis with anti-Ras (Ras), anti-p120RasGAP (p120RasGAP), and anti–β-tubulin (β-tubulin) antibodies as indicated at the left. (B) Serum-starved C2C12 myoblasts transfected with siRNA as described in A were stimulated for 10 min with or without 10 nM IGF-I in the absence or presence of 1.7 or 3.4 nM ephrinA1-Fc (A1-Fc) as indicated at the top. Cell lysates were subjected to Western blot analysis with anti–phospho-ERK1/2 (p-ERK1/2), anti-ERK1/2 (ERK1/2), anti–phospho-AKT (p-AKT), anti-AKT (AKT), and anti-p120RasGAP (p120RasGAP) antibodies as indicated at the left. (C) Phosphorylation levels of ERK1/2 (top) and AKT (bottom) observed in B were quantified and represented by the ratio of phospho-ERK1/2 or phospho-AKT to total ERK1/2 or total AKT, respectively. Values are expressed as explained in the legend of Figure 1B. Values are expressed relative to the ratio obtained from the IGF-I–treated cells transfected with control siRNA. *$p < 0.05$, **$p < 0.01$, significant differences between two groups. N.S., no significance between two groups. a.u., arbitrary unit(s).

transcription (RT)–PCR analysis revealed that C2C12 myoblasts express multiple members of ephrinA ligands such as ephrinA1, ephrinA3, ephrinA4, and ephrinA5 and those of EphA receptors, which include EphA1, EphA2, EphA3, and EphA4 (Supplemental Figure S3), we decided to use a dominant-negative approach instead of performing siRNA-mediated silencing of ephrinA ligands and EphA receptors. We prepared the adenovirus encoding the EphA2 receptor mutant lacking the cytoplasmic region (EphA2Δcyto), which was previously reported to exhibit dominant-negative activity (Cheng *et al.*, 2003; Taddei *et al.*, 2009). Overexpression of EphA2Δcyto blunted the ephrinA1-Fc–mediated phosphorylation of EphA2 in C2C12 cells (Figure 6A). It is significant that phosphorylation of EphA2 was greater in the confluent C2C12 cells than in the sparse cells (Figure 6B). Phosphorylation of EphA2 was likely to be induced by the binding of EphA2 to endogenous ephrinA upon cell–cell contact. EphA2 phosphorylation observed in the confluent cells was decreased by overexpression of EphA2Δcyto (Figure 6B), indicating that the EphA2 signal functions under confluent culture conditions and can be blocked by overexpression of EphA2Δcyto. Because C2C12 cells express several members of the EphA receptor family, as indicated by RT-PCR analysis, it can be assumed that ephrinA1-Fc suppresses IGF-I–induced activation of ERK1/2 through multiple members of EphA receptors. In C2C12 and L6 myoblasts, the inhibitory effect of ephrinA1-Fc on ERK1/2 activation in response to IGF-I was canceled by overexpression of EphA2Δcyto (Figure 6C and Supplemental Figure S4), implying that EphA2Δcyto acts as a dominant-negative mutant not only for EphA2, but also for other members of the EphA receptor family.

Endogenous ephrinA/EphA signal is required for efficient myogenic differentiation induced by IGF-I

To clarify the role of the ephrinA/EphA signal in IGF-I–induced myogenic differentiation, the EphA signal was abrogated by EphA2Δcyto overexpression during IGF-I–induced myogenic differentiation. C2C12 and L6 myoblasts infected with adenoviruses encoding EphA2Δcyto exhibited decreased formation of MHC-positive myotubes compared to the uninfected cells or the cells infected with β-galactosidase (β-gal)–encoding adenoviruses (Figure 7, A and B, and Supplemental Figure S5A). Consistently, IGF-I–mediated expression of MHC protein was significantly reduced by EphA2Δcyto overexpression (Figure 7, C and D, and Supplemental Figure S5B).

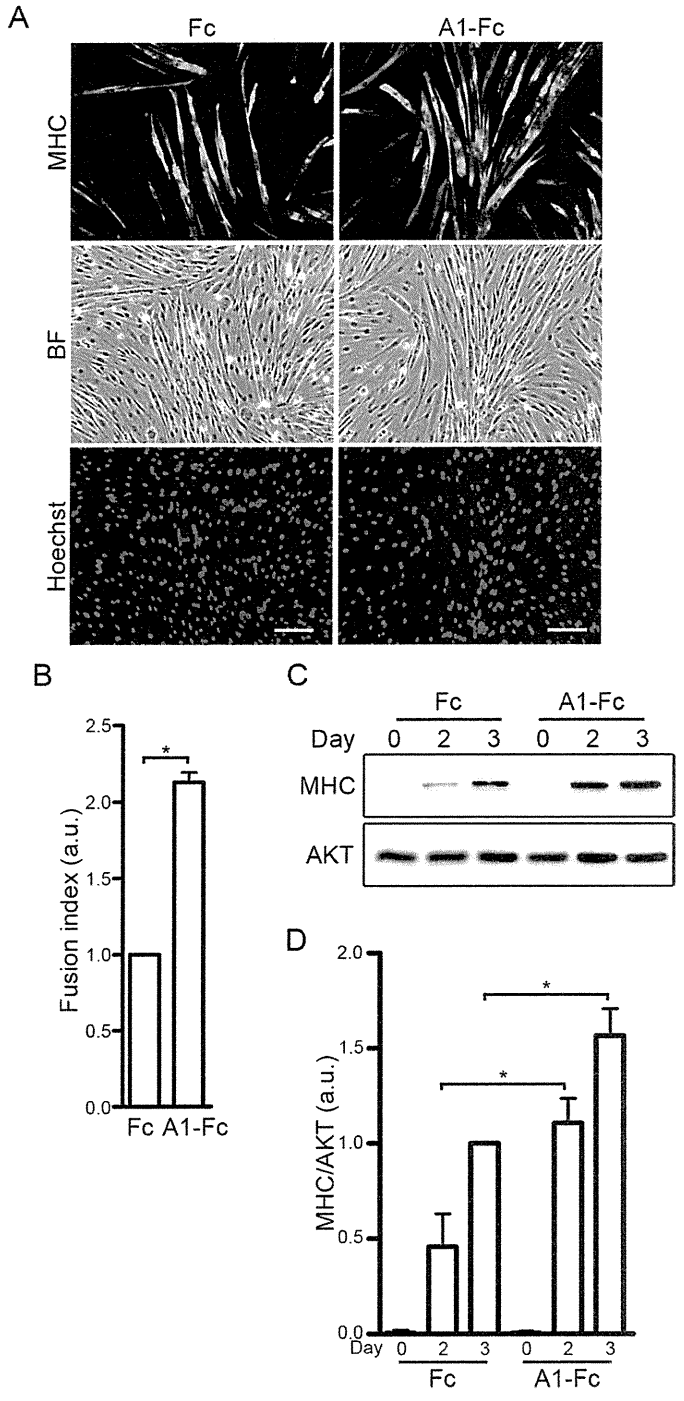

FIGURE 3: The ephrinA/EphA signal promotes IGF-I–induced myogenic differentiation. (A) Immunocytochemical analysis of C2C12 myoblasts using anti-MHC antibody. Confluent cells were differentiated into myotubes in DMEM containing 1% FBS and 10 nM IGF-I in the presence of either 6.4 nM Fc (Fc) or ephrinA1-Fc (A1-Fc) for 3 d. The cells were then fixed, immunostained with anti-MHC antibody, and visualized with Alexa Fluor 488–conjugated secondary antibody. The cells were also poststained with Hoechst 33342 to visualize the nuclei. Alexa 488 (MHC), bright-field (BF), and Hoechst 33342 (Hoechst) images are shown as indicated at the left. Experiments were repeated three times with similar results. Scale bars, 100 μm. (B) The fusion index observed in A was determined by dividing the number of nuclei within multinucleated myotubes by the total number of nuclei analyzed. Values are expressed relative to that observed in the cells differentiated in the presence of Fc and shown as means ± SD of three independent experiments. (C) Confluent C2C12 myoblasts were differentiated into myotubes in DMEM containing 1% FBS and 10 nM IGF-I in the presence of either 6.4 nM Fc (Fc) or ephrinA1-Fc (A1-Fc) for time periods (days) indicated at the top. Cell lysates were subjected to Western blot analysis using anti-MHC (MHC) and anti-AKT (AKT) antibodies as indicated at the left. (D) The expression level of MHC observed in C was quantified by normalizing the expression of MHC by that of AKT. Values are expressed relative to that observed in the cells differentiated in the presence of Fc for 3 d and shown as means ± SD of three independent experiments. *$p < 0.05$, significant differences between two groups. a.u., arbitrary unit(s).

These findings indicate that the ephrinA/EphA signal is required for efficient myogenic differentiation induced by IGF-I in myoblast cell lines.

To investigate whether myogenic differentiation induced by IGF-I requires the suppression of ERK1/2 activity by the ephrinA/EphA signal, we first examined the effect of EphA2Δcyto overexpression on ERK1/2 activity by inducing differentiation with IGF-I. The ERK1/2 activity of the C2C12 cells expressing EphA2Δcyto varied at the several time points during differentiation and was not always significantly increased compared with either the parental cells or those expressing β-gal. Therefore, to further assess the effect of EphA2Δcyto on the ERK1/2 activity during the differentiation, we examined it using the cells in the presence of ephrinA1-Fc in addition to IGF-1. C2C12 cells infected with adenoviruses expressing EphA2Δcyto exhibited a high level of ERK1/2 activity compared to those infected without or with β-gal–expressing adenoviruses during myogenic differentiation (Supplemental Figure S6). Furthermore, we investigated the effect of a MEK1/2 inhibitor, U0126, on the IGF-I–induced myogenic differentiation. U0126 slightly enhanced formation of MHC-positive myotubes and increased the expression of MHC in C2C12 and L6 myoblasts infected with or without β-gal–encoding adenoviruses (Figure 8 and Supplemental Figure S5). As observed in Figure 7, overexpression of EphA2Δcyto partially inhibited myotube formation and decreased the expression of MHC (Figure 8 and Supplemental Figure S5). However, the inhibitory effect of EphA2Δcyto on IGF-I-mediated myogenic differentiation was completely suppressed by the treatment with U0126 (Figure 8 and Supplemental Figure S5). Collectively, these findings suggest that IGF-I–induced myogenic differentiation is facilitated by the ephrinA/EphA signal, leading to down-regulation of the ERK1/2 cascade in myoblast cell lines.

DISCUSSION

In the present study, we investigated the role of ephrin/Eph signaling in skeletal muscle differentiation and found that the ephrinA/EphA signal facilitates IGF-I–induced myogenic differentiation by repressing the Ras–ERK1/2 signaling cascade through p120RasGAP in myoblast cell lines (Figure 9). To our knowledge, this study reveals for the first time the potential role of the ephrinA/EphA signal in skeletal myogenesis.

We delineated the molecular mechanism by which an endogenous ephrinA/EphA signal is involved in the inactivation of ERK1/2 that is preferable for myogenic differentiation induced by IGF-I. Although it is well known that IGFs promote myogenic differentiation through the PI3K/AKT pathway, IGFs also induces activation of myogenic inhibitory signal mediated by the ERK1/2. Activation of the PI3K/AKT pathway is responsible for myogenic differentiation, whereas the ERK1/2 pathway counteracts the PI3K/AKT pathway–dependent myogenic differentiation (Kaliman *et al.*, 1996, 1998; Bennett and Tonks, 1997; Coolican *et al.*, 1997; Tortorella *et al.*,

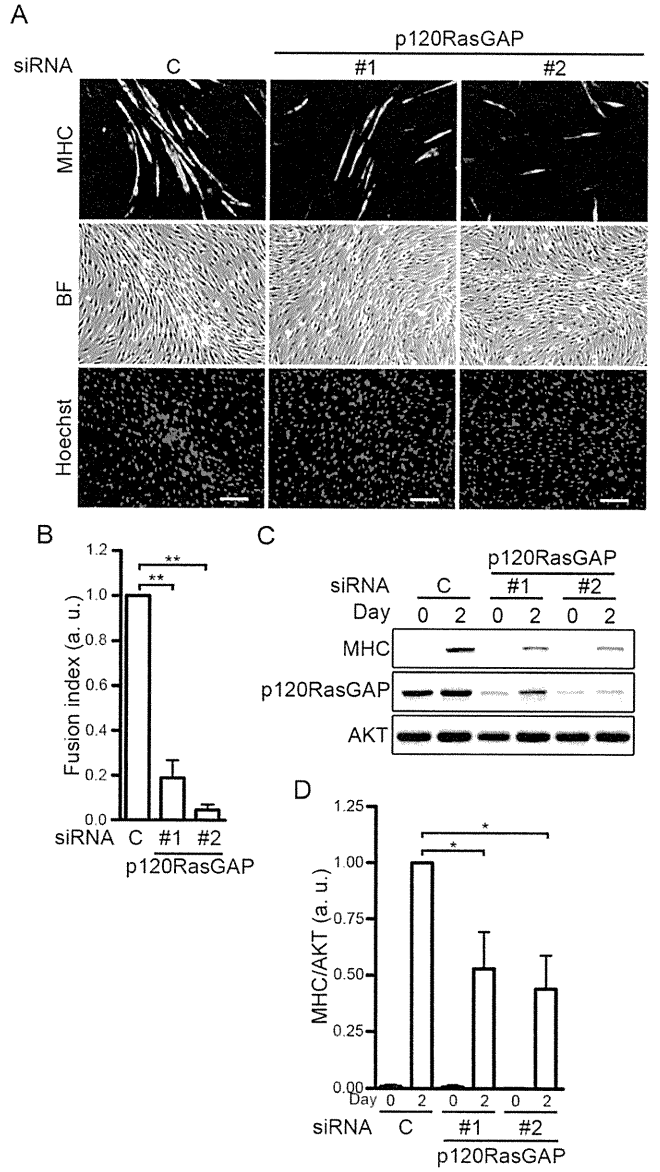

FIGURE 4: The ephrinA/EphA signal promotes IGF-I–dependent myogenic differentiation through p120RasGAP. (A) C2C12 myoblasts transfected with either control siRNA (C) or two independent siRNAs targeting p120RasGAP (1 and 2) were differentiated into myotubes in DMEM containing 1% FBS and 10 nM IGF-I in the presence of 6.4 nM ephrinA1-Fc for 2 d. The cells were immunostained with anti-MHC antibody and visualized with Alexa Fluor 488–conjugated secondary antibody. The cells were also poststained with Hoechst 33342 to visualize the nuclei. Alexa 488 (MHC), bright-field (BF), and Hoechst 33342 (Hoechst) images are shown as indicated at the left. Experiments were repeated three times with similar results. Scale bars, 100 μm. (B) The fusion index observed in A was determined as described in the legend of Figure 3B. Values are expressed relative to that observed in the cells transfected with control siRNA and shown as means ± SD of three independent experiments. (C) siRNA-transfected C2C12 myoblasts were differentiated into myotubes as described in A for time periods (days) indicated at the top. Cell lysates were subjected to Western blot analysis using anti-MHC (MHC), anti-p120RasGAP (p120RasGAP), and anti-AKT (AKT) antibodies as indicated at the left. (D) Expression level of MHC observed in C was quantified by normalizing the expression of MHC by that of AKT. Values are expressed relative to that observed in the control siRNA-transfected cells differentiated for 2 d and shown as means ± SD of three independent experiments. *$p < 0.05$, **$p < 0.01$, significant differences between two groups. a.u., arbitrary unit(s).

2001; de Alvaro *et al.*, 2005; Koyama *et al.*, 2008). Thus it is reasonable that the mechanisms that suppress the ERK1/2 pathway might exist to facilitate myogenic differentiation during skeletal myogenesis.

The EphrinA/EphA signal in C2C12 cells suppresses ERK1/2 during myogenesis. EphA and EphB receptors inhibit the Ras–ERK1/2 pathway by decreasing the Ras activity through p120RasGAP in various types of cells (Elowe *et al.*, 2001; Miao *et al.*, 2001; Tong *et al.*, 2003; Parri *et al.*, 2005; Pasquale, 2010). Thus, we assumed that the ephrin/Eph signal is favorable for skeletal myogenesis and found that the ephrinA/EphA signal down-regulates the Ras–ERK1/2 pathway induced by IGF-I through p120RasGAP in myoblast cell lines, thereby facilitating myogenic differentiation. In addition, it was previously reported that DA-Raf1, a splicing isoform of A-Raf, is expressed during skeletal myogenesis and enhances myogenic differentiation of C2C12 cells by acting as a dominant-negative antagonist of the Ras–ERK1/2 pathway (Yokoyama *et al.*, 2007). Recently glypican, a heparin sulfate proteoglycan expressed in myoblasts, was reported to sequester basic fibroblast growth factor (bFGF) in lipid rafts away from its receptors (Gutierrez and Brandan, 2010). Because bFGF represses myogenic differentiation through the activation of the ERK1/2 pathway (Tortorella *et al.*, 2001), sequestration of bFGF by glypican promotes myogenic differentiation. Therefore the ERK1/2 activity in myoblasts is suppressed by various mechanisms to facilitate myogenic differentiation during skeletal myogenesis.

Temporal ERK1/2 inactivation and activation might be important for myogenesis. The ERK1/2 cascade is essential for proliferation of myoblasts but negatively regulates myogenic differentiation by suppressing the expression of muscle-specific genes. Of interest, it was also shown that the late stage of skeletal muscle differentiation requires the ERK1/2 activity (Bennett and Tonks, 1997). Expression of MAPK phosphatase-1, which inhibits ERK1/2 activity, is down-regulated during the late stage of myogenesis, and its overexpression prevents myotube formation without affecting the expression of muscle-specific genes. Thus the ERK1/2 activity is temporarily controlled during myogenic differentiation. On induction of myogenic differentiation, the cell–cell contact–dependent ephrinA/EphA signal suppresses ERK1/2 activity, as we demonstrated in this study. However, the ephrinA/EphA signal may be down-regulated to reactivate the ERK1/2 cascade at the late stage of skeletal muscle differentiation. Because EphA2 expression is induced by activation of the Ras–ERK1/2 pathway (Macrae *et al.*, 2005), EphA-signal–dependent inhibition of the Ras–ERK1/2 pathway may lead to down-regulation of EphA2 expression. Therefore the ERK1/2 activity may be temporarily controlled by an EphA2–Ras–ERK1/2 negative feedback loop during skeletal myogenesis.

There is only limited information on the role of the ephrin/Eph signal in muscle development. It was shown that the ephrinA5/EphA4 signal is involved in migration of muscle precursor cells (Swartz *et al.*, 2001). EphrinA5 expressed in mesoderm tissue prevents EphA4-positive muscle precursor cells from migrating into abnormal embryonic regions. Furthermore, a role of EphA4 signal in maintenance of neuromuscular junctions was suggested (Lai *et al.*, 2004). EphA4 localized at the neuromuscular junctions of adult muscle induces expression of acetylcholinesterase, an enzyme that degrades the neurotransmitter acetylcholine, through Janus kinase/signal transducers and activators of transcription pathway. However, the role of ephrin/Eph signal in differentiation of myoblasts into myocytes has never been reported. Therefore the present study is the first to unravel the potential role of the ephrinA/EphA signal in myogenic differentiation of myoblast cell lines. However, further study is required to clarify whether the ephrinA/EphA signal is

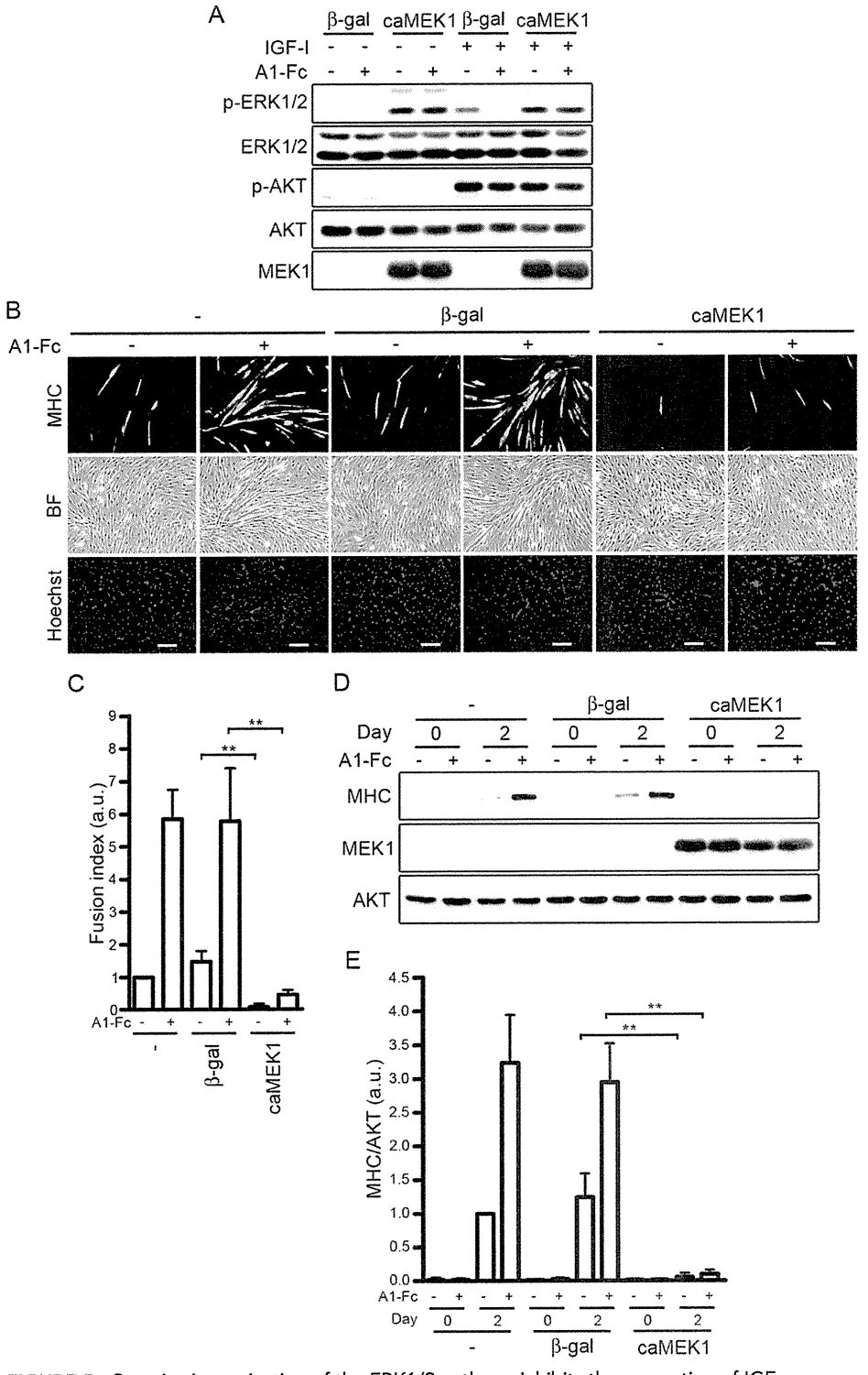

FIGURE 5: Constitutive activation of the ERK1/2 pathway inhibits the promotion of IGF-I–mediated myogenic differentiation by the ephrinA/EphA signal. (A) Serum-starved C2C12 myoblasts infected with adenoviruses encoding either β-gal (β-gal) or constitutive active mutant of MEK1 (caMEK1) were stimulated with or without 10 nM IGF-I for 10 min in the presence of 1.7 nM Fc (–) or ephrinA1-Fc (A1-Fc) as indicated at the top. Cell lysates were subjected to Western blot analysis with anti–phospho-ERK1/2 (p-ERK1/2), anti-ERK1/2 (ERK1/2), anti–phospho-AKT (p-AKT), anti-AKT (AKT), and MEK1 (MEK1) antibodies as indicated at the left. (B) C2C12 myoblasts infected without (–) or with adenoviruses encoding either β-gal (β-gal) or constitutive active mutant of MEK1 (caMEK1) were differentiated into myotubes in DMEM containing 1% FBS and 10 nM IGF-I in the presence of 6.4 nM Fc (–) or ephrinA1-Fc (A1-Fc) for 2 d. The cells were immunostained with anti-MHC antibody, and visualized with Alexa Fluor 488–conjugated secondary antibody. The cells were also poststained with Hoechst 33342 to visualize the nuclei. Alexa 488 (MHC), bright-field (BF), and Hoechst 33342 (Hoechst) images are shown as indicated at the left. Experiments were repeated three times with similar results. Scale bars, 100 μm. (C) The fusion index observed in B was determined as described in the legend of Figure 3B. Values are expressed relative to that observed in the uninfected cells differentiated in the presence of Fc and shown as means ± SD of three independent experiments. (D) Adenovirus-infected C2C12 myoblasts were differentiated into myotubes as described in B for time periods (days) indicated at the top. Cell lysates were subjected to Western blot analysis using anti-MHC (MHC), anti-MEK1 (MEK1), and anti-AKT (AKT) antibodies as indicated at the left. (E) The expression level of MHC observed in D was quantified by normalizing the expression of MHC by that of AKT. Values are expressed relative to that observed in the uninfected cells differentiated in the presence of Fc for 2 d and shown as means ± SD of three independent experiments. **$p < 0.01$, significant differences between two groups. a.u., arbitrary unit(s).

implicated in differentiation of primary myoblasts or in myogenic differentiation in vivo.

The present study apparently indicates that p120RasGAP-mediated inhibition of the Ras–ERK1/2 pathway is responsible for the promotion of myogenic differentiation by the ephrinA/EphA signal in myoblast cell lines. However, since the ephrinA/EphA signal not only activates p120RasGAP but also stimulates various intracellular signaling molecules (Pasquale, 2010), myogenic differentiation might also be regulated by other signaling pathways. EphA2 signaling is known to promote the intercellular junctions mediated by cadherins such as E-cadherin and N-cadherin (Miao *et al.*, 2003; Cooper *et al.*, 2008; Jun *et al.*, 2009; Miura *et al.*, 2009). Because engagement of N-cadherin and M-cadherin leads to the activation of promyogenic signaling pathways in myoblasts (Krauss, 2010), the ephrinA/EphA signal may promote skeletal myogenesis by enhancing cadherin-based cell–cell junctions. RhoA is activated by EphA receptors through ephexin (Shamah *et al.*, 2001) and induces expression of muscle-specific genes through serum response factor (Carnac *et al.*, 1998). Thus the ephrinA/EphA signal may also regulate myogenesis through RhoA-dependent expression of muscle-specific genes. In addition, it has been shown that ephrinA-mediated reverse signaling also regulates various biological functions, such as insulin secretion from β cells, neurogenesis, tumor suppression, and tumor progression (Pasquale, 2010). Thus it would be interesting to examine the involvement of ephrinA reverse signaling in myogenic differentiation.

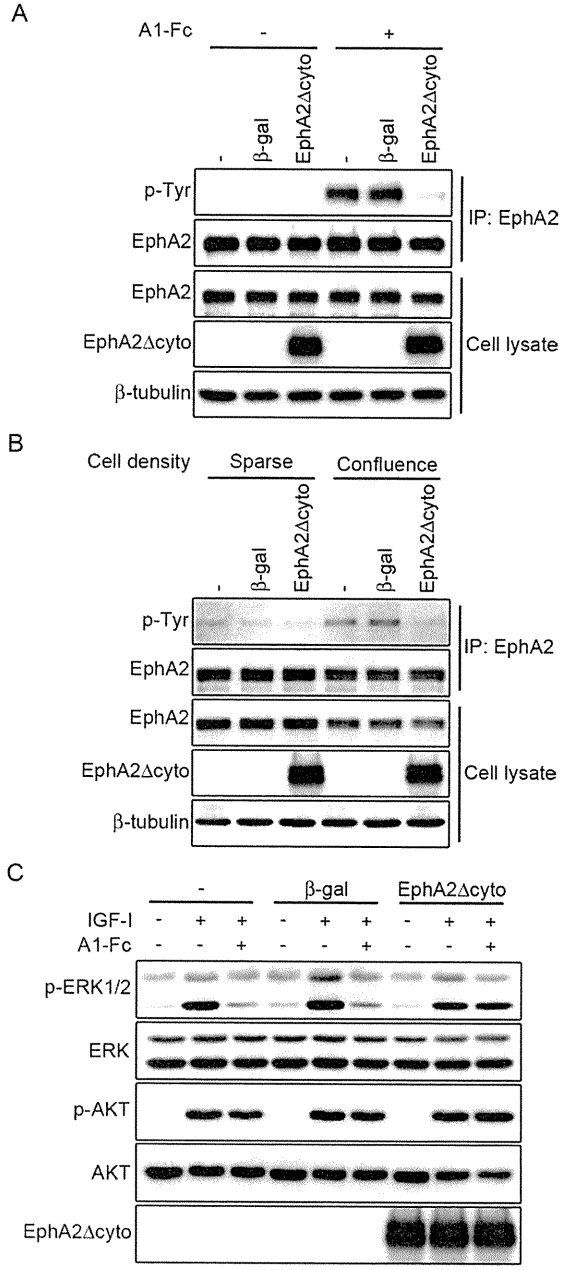

FIGURE 6: EphA2 mutant lacking the cytoplasmic region acts as a dominant-negative EphA receptor. (A) C2C12 myoblasts infected without (–) or with adenoviruses encoding either β-gal (β-gal) or C-terminal HA-tagged EphA2 mutant that lacks the cytoplasmic region (EphA2Δcyto) were serum starved and stimulated for 10 min in the presence of 2.2 nM Fc (–) or ephrinA1-Fc (A1-Fc) as indicated at the top. EphA2 was immunoprecipitated with anti-EphA2 antibody and subjected to Western blot analysis with anti-phosphotyrosine (p-Tyr) and anti-EphA2 (EphA2) antibodies. Aliquots of total-cell lysate were also subjected to Western blot analysis with anti-EphA2 (EphA2), anti-HA (EphA2Δcyto), and anti–β-tubulin (β-tubulin) antibodies as indicated at the left. (B) C2C12 myoblasts infected with adenoviruses as described in A were placed on the culture dishes for 4 h under either sparse or confluent culture condition as indicated at the top. Immunoprecipitation of EphA2 and Western blot analysis were performed as described in A. (C) C2C12 myoblasts infected with adenoviruses as described in A were serum starved and stimulated for 10 min with or without 10 nM IGF-I in the presence of 1.7 nM Fc (–) or ephrinA1-Fc (A1-Fc) as indicated at the top. Cell lysates were subjected to Western blot analysis with anti–phospho-ERK1/2 (p-ERK1/2), anti-ERK1/2 (ERK1/2), anti–phospho-AKT (p-AKT), anti-AKT (AKT), and anti-HA (EphA2Δcyto) antibodies as indicated at the left.

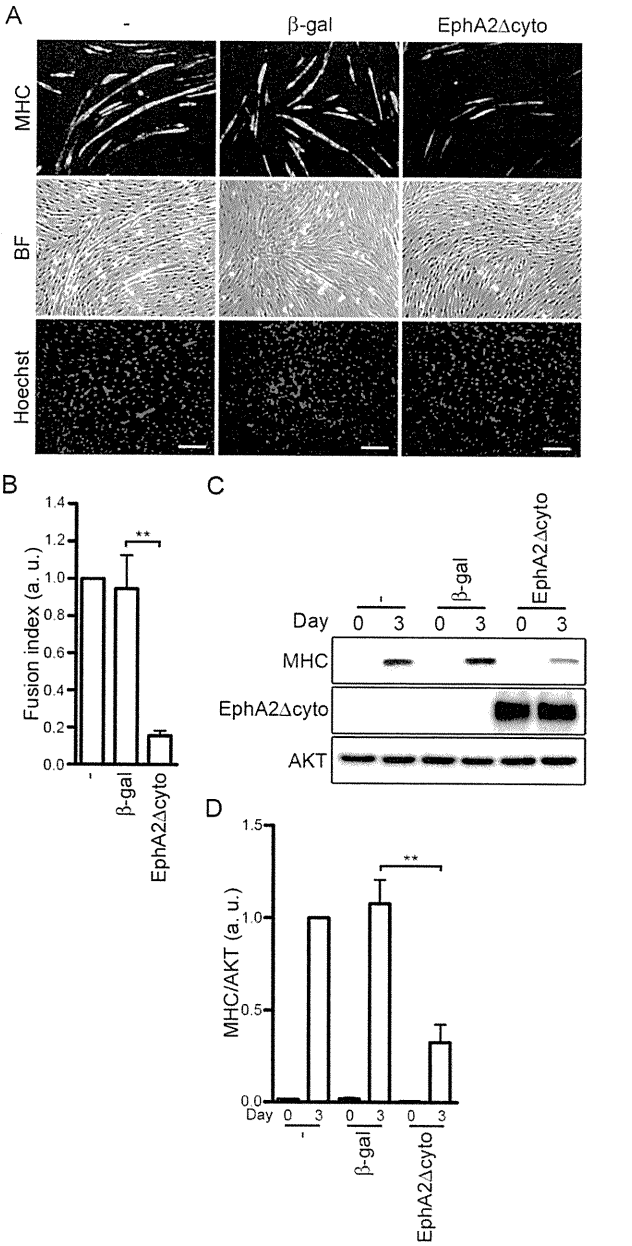

FIGURE 7: IGF-I–induced myogenic differentiation is blunted by blocking the ephrinA/EphA signal. (A) C2C12 myoblasts infected without (–) or with adenoviruses encoding either β-gal or EphA2Δcyto were differentiated into myotubes in DMEM containing 1% FBS and 10 nM IGF-I for 3 d. The cells were immunostained with anti-MHC antibody and visualized with Alexa Fluor 488–conjugated secondary antibody. The cells were also poststained with Hoechst 33342 to visualize the nuclei. Alexa 488 (MHC), bright-field (BF), and Hoechst 33342 (Hoechst) images are shown as indicated at the left. Experiments were repeated three times with similar results. Scale bars, 100 μm. (B) The fusion index observed in A was determined as described in the legend of Figure 3B. Values are expressed relative to that observed in the uninfected cells and shown as means ± SD of three independent experiments. (C) Adenovirus-infected C2C12 myoblasts were differentiated into myotubes as described in A for time periods (days) indicated at the top. Cell lysates were subjected to Western blot analysis using anti-MHC (MHC), anti-HA (EphA2Δcyto), and anti-AKT (AKT) antibodies as indicated at the left. (D) The expression level of MHC observed in C was quantified by normalizing the expression of MHC by that of AKT. Values are expressed relative to that observed in the uninfected cells differentiated for 3 d and shown as means ± SD of three independent experiments. **$p < 0.01$, significant differences between two groups. a.u., arbitrary unit(s).

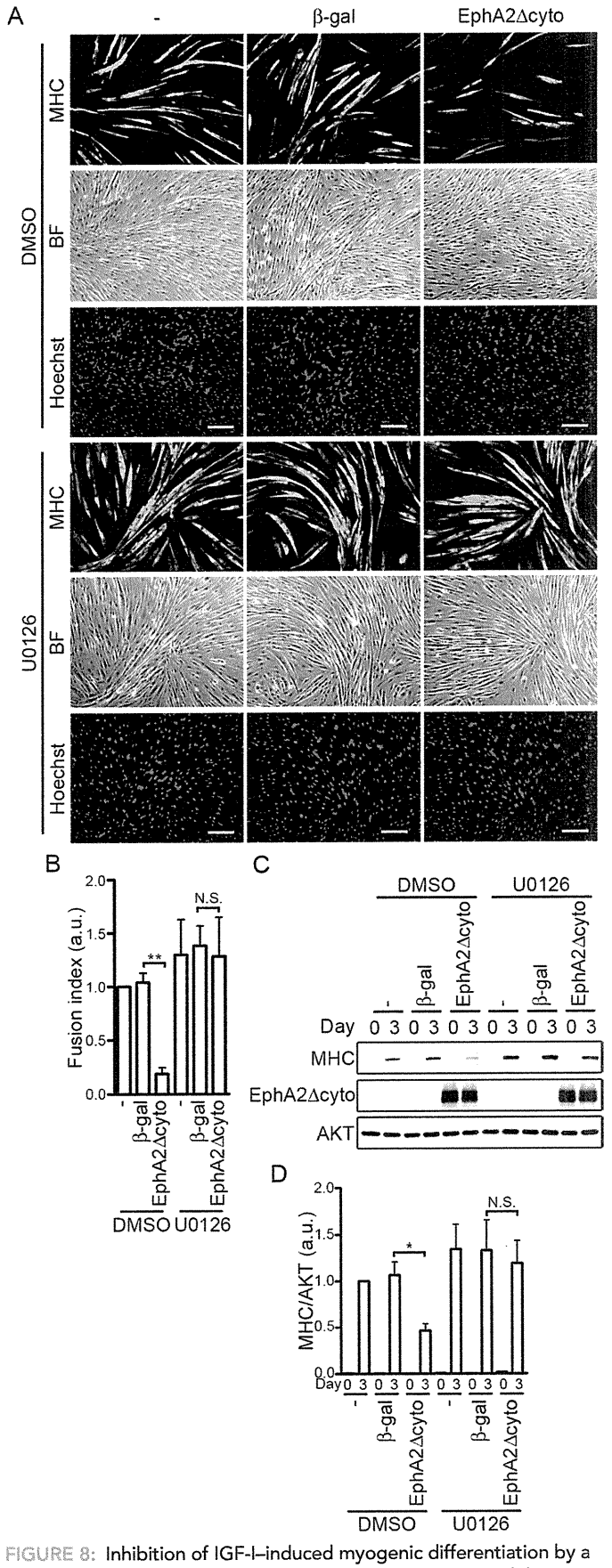

FIGURE 8: Inhibition of IGF-I–induced myogenic differentiation by a dominant-negative EphA receptor mutant is canceled by inhibiting the ERK1/2 pathway. (A) C2C12 myoblasts infected without (–) or with adenoviruses encoding either β-gal or EphA2Δcyto were differentiated into myotubes in DMEM containing 1% FBS and 10 nM IGF-I in the presence of vehicle (dimethyl sulfoxide [DMSO]) or 3 μM U0126 for 3 d. The cells were immunostained with anti-MHC antibody and visualized with Alexa Fluor 488–conjugated secondary antibody. The cells were also poststained with Hoechst 33342 to visualize the nuclei. Alexa 488 (MHC), bright-field (BF), and Hoechst 33342 (Hoechst) images are shown as indicated at the left. Experiments were repeated three times with similar results. Scale bars, 100 μm. (B) The fusion index observed in A was determined as described in the legend of Figure 3B. Values are expressed relative to that observed in the uninfected cells differentiated in the presence of DMSO and shown as means ± SD of three independent experiments. (C) Adenovirus-infected C2C12 myoblasts were differentiated into myotubes as described in A for time periods (days) indicated at the top. Cell lysates were subjected to Western blot analysis using anti-MHC (MHC), anti-HA (EphA2Δcyto), and anti-AKT (AKT) antibodies as indicated at the left. (D) The expression level of MHC observed in C was quantified by normalizing the expression of MHC by that of AKT. Values are expressed relative to that observed in the uninfected cells differentiated in the presence of DMSO for 3 d and shown as means ± SD of three independent experiments. *$p < 0.05$, **$p < 0.01$, significant differences between two groups. N.S., no significance between two groups. a.u., arbitrary unit(s).

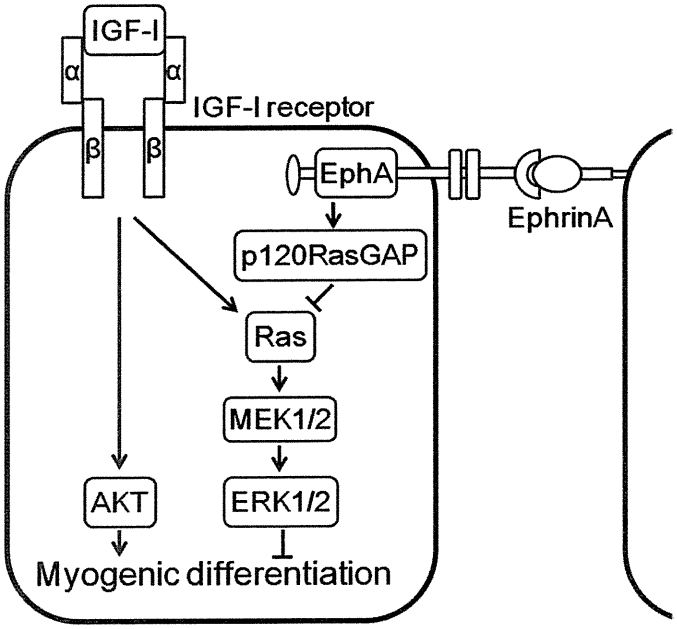

FIGURE 9: Schematic representation of a proposed model for how the ephrinA/EphA signal potentiates IGF-I–induced myogenic differentiation. IGF-I not only induces myogenic differentiation through the PI3K/AKT pathway but also stimulates the myogenic inhibitory signal mediated by the Ras–ERK1/2 cascade. The cell–cell contact–dependent ephrinA/EphA signal suppresses the RasxERK1/2 cascade by IGF-I through p120RasGAP, thereby facilitating IGF-I–mediated myogenic differentiation.

In conclusion, we have demonstrated that the cell–cell contact–dependent ephrinA/EphA signal suppresses IGF-I–induced activation of the Ras–ERK1/2 cascade by decreasing the Ras activity through p120RasGAP in myoblast cell lines. This molecular mechanism accounts for IGF-I–induced myogenic differentiation facilitated by ephrinA/EphA.

MATERIALS AND METHODS

Reagents and antibodies

COMP-Ang1 was kindly provided by G. Y. Koh (Korea Advanced Institute of Science and Technology, Daejeon, South Korea). Human

recombinant IGF-I was kindly provided by Astellas Pharma (Tokyo, Japan). Other reagents were purchased as follows: Hoechst 33342 nuclear dye from Sigma-Aldrich (St. Louis, MO); human Fc, mouse ephrinA1-Fc, and mouse ephrinB1-Fc from R&D Systems (Minneapolis, MN); and U0126 from Cell Signaling Technology (Beverly, MA). Antibodies were purchased as follows: anti–phospho-p44/42 ERK1/2 (Thr-202/Tyr-204), anti–phospho-AKT (Thr-308), and anti-AKT from Cell Signaling Technology; anti-MEK1, anti-ERK1/2, anti-EphA2, and anti-phosphotyrosine (PY99) from Santa Cruz Biotechnology (Santa Cruz, CA); anti-HA tag from Roche Diagnostics (Indianapolis, IN); anti–pan Ras from Calbiochem (La Jolla, CA); anti-MHC (MF20) from the Developmental Studies Hybridoma Bank (Iowa City, IA); anti–β-tubulin from Sigma-Aldrich; horseradish peroxidase–conjugated anti-mouse, anti-rabbit, and anti-rat from GE Healthcare Life Sciences (Piscataway, NJ); and Alexa Fluor 488–labeled goat anti–mouse IgG from Molecular Probes (Eugene, OR).

Cell culture, stimulation, and myogenic differentiation

Mouse C2C12 and rat L6 myoblasts were maintained as subconfluent monolayers in DMEM (Nissui, Tokyo, Japan) supplemented with FBS (20% for C2C12 cells, 10% for L6 cells), 4.5 g/l glucose, 0.58 g/l L-glutamine, 100 U/ml penicillin, and 100 μg/ml streptomycin. To examine the IGF-I–induced activation of ERK1/2, AKT, and Ras, the cells were serum starved overnight and stimulated with IGF-I in the presence or absence of nonclustered Fc, ephrinA1-Fc, or ephrinB1-Fc as indicated in the figure legends. For the induction of myogenic differentiation, cultured medium was replaced with DMEM containing 1% FBS and IGF-I at the concentrations described in the figure legends, when cell density reached confluency. The differentiation medium was exchanged every day. Human umbilical vein endothelial cells were purchased from Kurabo (Osaka, Japan) and maintained as described previously (Fukuhara *et al.*, 2005).

siRNA-mediated protein knockdown

Stealth siRNAs targeting mouse p120RasGAP (no. 1, 5′-UGUCCAACACCUAACAACCAGUUUA-3′; no. 2, 5′-CACUACUGGCCAGCAUCCUACUAAA-3′) and siRNA duplexes with irrelevant sequences (Stealth RNAi negative control) as a control were purchased from Invitrogen (Carlsbad, CA). For siRNA-mediated gene silencing, 10 nM siRNA duplexes were introduced into C2C12 myoblasts by reverse transfection using Lipofectamine RNAiMAX reagent (Invitrogen) according to the manufacturer's instruction. The cells were replated 24–30 h after the transfection and subjected to the experiments.

Adenovirus vector construction and infection

To generate adenovirus vector expressing the human EphA2 mutant that lacks the cytoplasmic region (EphA2Δcyto), a cDNA fragment encoding amino acids 1–574 of human EphA2 was amplified by PCR using an expression vector for human EphA2 (a gift from A. Sakakibara, Nagoya University, Nagoya, Japan) as a template and was subcloned into pCMV-HA vector (Fukuhara *et al.*, 2008). Then, a cDNA fragment encoding C-terminal HA-tagged EphA2Δcyto was excised and inserted into the pShuttle vector (Clontech, Mountain View, CA). The adenovirus was produced by using the Adeno-X system according to the manufacturer's protocol (Clontech). Recombinant adenovirus vectors encoding β-gal and caMEK1 were kindly provided by M. Matsuda (Kyoto University, Kyoto, Japan) and S. Kawashima (Kobe University, Kobe, Japan), respectively. For adenoviral infection, subconfluent C2C12 cells were infected with adenoviruses at the multiplicity of infection of 30 for 24 h and replated for the experiments.

Immunoprecipitation and Western blot analysis

Cells were washed with ice-cold phosphate-buffered saline (PBS), lysed in lysis buffer containing 50 mM Tris, pH 7.5, 150 mM NaCl, 1 mM sodium orthovanadate, 20 mM sodium fluoride, 1% Nonidet P-40, 0.1% SDS, 0.5% sodium deoxycholate, and 1× protease inhibitor cocktail (Roche Diagnostics), and centrifuged at 15,000 × *g* for 20 min at 4°C. The supernatant was used as precleared total-cell lysate. For the immunoprecipitation of EphA2, the cells were lysed in lysis buffer containing 20 mM Tris, pH 7.5, 150 mM NaCl, 3 mM EDTA, 1% Nonidet P-40, and 1× protease inhibitor cocktail. EphA2 was immunoprecipitated from the cleared lysates by incubation with anti-EphA2 antibody for 2 h at 4°C. Immunocomplexes were recovered with the aid of protein A–Sepharose beads (GE Healthcare Life Sciences). Aliquots of cell lysate and the immunoprecipitates were subjected to SDS–PAGE and Western blot analysis with the antibodies as indicated in the figure legends.

Immunocytochemistry

Cells plated on 3.5-cm collagen type I–coated plastic dishes (Iwaki Asahi Glass, Tokyo, Japan) were fixed with 2% formaldehyde in PBS for 15 min, permeabilized with 0.1% Triton X-100 for 5 min, and blocked with PBS containing 4% bovine serum albumin for 1 h. The cells were then stained with anti-MHC antibody for 1 h at room temperature. Protein reacting with the antibody was visualized with Alexa Fluor 488–conjugated secondary antibody. The nucleus was also poststained with Hoechst 33342 nuclear dye. Fluorescent images of Alexa Fluor 488 and Hoechst 33342 and phase-contrast images were recorded with an Olympus IX-81 inverted fluorescence microscope (Olympus Corporation, Tokyo, Japan) as described previously (Noda *et al.*, 2010).

Reverse transcription-PCR

Total RNA was prepared from C2C12 myoblasts using TRIzol reagent (Invitrogen), and reverse-transcribed by random hexamer primers using Superscript II (Invitrogen) according to the manufacturer's instruction. PCR was performed using the gene-specific primers listed in the Supplemental Table S1. Amplification of glyceraldehyde-3-phosphate dehydrogenase was also performed in parallel as a control.

Detection of GTP-bound form of Ras

Ras activation was assessed using a pull-down technique. Cells were lysed at 4°C in a pull-down lysis buffer containing 20 mM Tris, pH 7.5, 100 mM NaCl, 10 mM $MgCl_2$, 1% Triton X-100, 1 mM ethylene glycol tetraacetic acid, 1 mM dithiothreitol, 1 mM sodium orthovanadate, and 1× protease inhibitor cocktail. GTP-bound Ras was collected on the glutathione transferase-tagged Ras binding domain of Raf precoupled to glutathione-Sepharose beads. GTP-bound Ras and aliquots of total cell lysate were subjected to Western blot analysis with the antibodies as indicated in the figure legends.

Statistical analysis

The signal intensity of the band of Western blot analysis was calculated using Scion Image software. All data are expressed as means ± SD. Differences among multiple groups were compared by one-way analysis of variance followed by a post hoc comparison tested with the Bonferroni method. Values of $p < 0.05$ were considered significant.

ACKNOWLEDGMENTS

We are grateful to G. Y. Koh (Korea Advanced Institute of Science and Technology) for COMP-Ang1, to A. Sakakibara (Nagoya University) for an expression vector for human EphA2, and to M. Matsuda